nature communications

Article | Article in Press

https://doi.org/10.1038/s41467-026-77034-w

ERα Micromap (μMap) proximity labeling reveals fulvestrant mechanisms

Received: 6 October 2025

Accepted: 28 July 2026

Published online: 31 August 2026

Check for updates

Chun Li[1,2,6], Zihan Dong[1,2,6], Romain O. Georges[3], Kristina Danga[3], Ciaran P. Seath[1,2,5], Yuka Amako[4], Jack L. Sloane[4], Aya M. Kelly[4], Joel W. Thompson[3] ✉ & David W. C. MacMillan[1,2] ✉

Estrogen Receptor alpha (ERα) is the primary driver in ER+ breast cancer and can be targeted using small molecules such as fulvestrant, a selective estrogen receptor degrader (SERD). Despite being approved over two decades ago and used regularly in post-menopausal women, its precise anti-tumor mechanism remains unclear, with several reports showing efficacy without the requirement for ERα degradation. To investigate the molecular basis of fulvestrant's action, we employed split intein-based μMap photo-proximity labeling to profile ERα-associated interactions. Our findings reveal that fulvestrant displaces oncogenic interactions induced by estradiol and promotes ERα translocation to promyelocytic leukemia (PML) nuclear bodies, leading to altered transcriptional signatures and senescence. Overall, this study offers insights into SERD mechanism of action and establishes a framework for evaluating additional ERα modulators and degraders.

Understanding the mechanism of action (MoA) of bioactive small molecules is pivotal in modern drug discovery and development, allowing for predictable drug efficacy and safety in later clinical stages[1,2]. Determining the molecular basis of ligand function not only enhances its probability of success in clinical trials[3], but also provides valuable insights for future target-based drug development[4], possible drug repurposing[5,6], and informed combination therapies[7]. Despite these advantages and the clear clinical need, the MoA of many approved drugs and clinical candidates remains incompletely understood.

One class of clinical molecules without a well-defined mechanism is the selective estrogen receptor degraders (SERDs), which are frequently used for treating patients with estrogen receptor positive (ER+) breast cancer[8]. Fulvestrant (Fulv), the first-in-class SERD approved by the FDA in 2002, is commonly prescribed to postmenopausal ER+ patients and has led to positive clinical outcomes[9]. Yet due to its requirement of painful and frequent intramuscular administration, oral replacements are highly sought after[10]. Fulv and other SERDs are considered hormone therapies that act by targeting the hormone receptor estrogen receptor alpha (ERα) and leading to its degradation[8]. However, drug candidates with excellent ERα degradation profiles and physiochemical properties do not necessarily demonstrate superior tumor suppression effects in vitro, in pre-clinical models, or in clinical trials. Several SERDs, including amcenestrant, GDC-0810, and AZD-9496, entered clinical trials yet were terminated during development due to lack of efficacy[11–15]. While clinical trial outcomes are shaped by many factors, this finding raises questions of whether the anti-tumor activity of SERDs arises from additional factors beyond ERα degradation. It was recently proposed that Fulv and other SERDs induce ERα intra-nuclear immobility, leading to suppressed transcriptional activity and increased protein turnover[16]. Despite advances in understanding Fulv function, the full molecular basis of its MoA remains to be determined.

ERα, as a nuclear receptor and a transcription factor, functions through binding dynamically to chromatin[17], other transcription factors[18,19], and remodeling complexes[20–22]. Estradiol (E2) is the natural ligand of ERα and facilitates the optimal loading of ERα homodimer onto DNA for its transcriptional activities[23]. E2-liganded ERα homodimer is able to rapidly move along the genome and interact with the palindromic estrogen response elements (ERE)[24,25], recruiting necessary co-activators for gene regulation[26]. In the presence of Fulv, ERα

[1]Merck Center for Catalysis at Princeton University, Princeton, NJ, USA. [2]Department of Chemistry, Princeton University, Princeton, NJ, USA. [3]Bristol Myers Squibb, San Diego, CA, USA. [4]Bristol Myers Squibb, Cambridge, MA, USA. [5]Present address: Cornell University, Ithaca, NY, USA. [6]These authors contributed equally: Chun Li, Zihan Dong. ✉e-mail: joel.thompson@bms.com; dmacmill@princeton.edu

shows greatly reduced mobility yet can still bind to ERE sites, albeit to a lesser extent[27]. Due to the highly transient nature of ERα, the accurate capture of its interactors requires a tool with high sensitivity and precise spatio-temporal control. In order to gain insight into the MoA of Fulv, we questioned whether we could use proximity labeling to probe the interactome of ERα, both in its native state and in response to small molecule antagonism. While both TurboID[28] and Biotinylation by Antibody Recognition (BAR)[29] have been utilized previously for the identification of ERα interactors, the ligand-dependent context has been relatively underexplored. To this end, we have leveraged our photocatalytic micromapping platform (μMap), which has been applied successfully to the precise mapping of protein–protein and small molecule–protein interactions in response to therapeutic stimuli[30–32]. The μMap technology deploys an iridium (Ir) photocatalyst and a short-lived carbene intermediate to achieve high-precision targeted labeling within a very small radius[33]. By establishing a comparative ERα μMap platform using the N-terminal split intein-based approach, we have uncovered a localization of Fulv-bound ERα in the nuclear condensate promyelocytic leukemia nuclear bodies (PML-NBs) via the bridging of chromatin remodeler ATRX (ATRX) and death-domain associated protein 6 (DAXX). We show that this change in localization leads to the displacement of E2-induced ERα transcriptional co-factors, ERα immobility, and the anti-tumor effects of Fulv. In PML-NBs, Fulv-bound ERα interacts strongly with chromatin, leading to hypophosphorylation of protein Rb and, subsequently, cellular senescence. Our study offers deeper insights into the mechanism of Fulv on ERα and provides a valuable resource to accelerate the development of next-generation SERD therapies.

Results

The ERα interactome is captured by μMap

To establish a platform for the ERα μMap, we adapted our previously reported split intein-based photo-proximity labeling system, which allows for the traceless incorporation of the photocatalyst to the protein of interest with minimal perturbation of the biological environment (Fig. 1a). The split intein system was originally developed to profile changes to the histone H2A interactome that occur upon addition of BRD2/3/4 targeting molecule JQ-1 and selective DOT1L methyltransferase inhibitor pinometostat. This was achieved by expressing the N-terminal fragment of the Cfa split intein (Cfa^N) with the protein of interest (POI) and conjugating the Ir photocatalyst to the C-terminal of Cfa split intein (Cfa^C). Through intein trans-splicing in whole nuclei, the Ir photocatalyst is installed onto the POI[32]. We anticipated that this platform would similarly prove amenable to the study of the drug-induced interactome changes of ERα (Fig. 1a). At the outset, the *ESR1*-HA-Cfa^N-FLAG construct was stably expressed in MCF7 cells. However, upon further evaluation of the biological activity of the fusion protein, we observed overall low protein levels and truncated expression (Supplementary Fig. 1a, b), despite its ability to achieve sufficient splicing with Cfa^C-Ir at concentrations as low as 0.3 μM (Supplementary Fig. 1c, d). The subsequent ERα μMap was also sub-optimal with both overall experimental depth and significant interactors lower than expected (Supplementary Fig. 1e–g, Supplementary Data 2). This phenomenon is possibly caused by the instability of a C-terminal ESR1 fusion as well as the relatively large size of the N-terminal Cfa split intein (12 kDa). As a result, an N-terminal intein-ERα fusion, utilizing the 4 kDa C-terminal Cfa split intein, was used instead for optimal results. We envisioned that the construct FLAG-Cfa^C-HA-*ESR1* could be applied in the pre-established split intein-based μMap with minimal alterations.

Upon stably expressing FLAG-Cfa^C-HA-*ESR1* into MCF7 cells, we observed adequate protein levels with no truncated product (Supplementary Fig. 2a). This construct functions similarly to endogenous ERα, undergoing modest degradation with the natural ligand estradiol (E2) and significant degradation with the therapeutically relevant ligand Fulv. This ligand-mediated ERα degradation can be rescued by the ubiquitin-activating enzyme (UAE) inhibitor, TAK-243, suggesting that the degradation is ubiquitin-dependent (Fig. 1c). Next, the iridium-based photocatalyst was appended onto a short GKGY peptide via PEG16 linker, which enabled conjugation with the purified Cfa^N through native chemical ligation (NCL) (Fig. 1b and Supplementary Fig. 2). The resulting Ir-Cfa^N permeates the nuclear membrane, allowing for the traceless incorporation of Ir catalyst onto ERα through intein trans-splicing at concentrations as low as 0.3 μM of Ir-Cfa^N after 1 h of end-to-end rotation at 37 °C (Fig. 1d). To validate the function of the splicing product, both wild-type (WT) MCF7 and FLAG-Cfa^C-HA-*ESR1*-expressing cells were treated with TAK-243 and E2 then subjected to the photolabeling workflow. Western blot analysis of all fractions along the process suggests successful incorporation of the Ir-photocatalyst onto the expressed construct. Notably, both endogenous ERα and the splicing product Ir-HA-*ESR1* were present in the elution fraction after streptavidin enrichment (Fig. 1e). Since ERα dimerizes upon E2 ligand binding, this labeling result is an indication of sufficient self-labeling as well as interactome-labeling. In addition, the expression level and pulldown of endogenous ERα suggests effective dimerization of Ir-bearing ERα with endogenous ERα, with minimal perturbation of ERα native function.

Having established the labeling system, we sought to leverage this platform for proteomic analysis. To evaluate the native ERα interactome, we first performed comparative proteomics between the treatments of E2 and DMSO (Fig. 1f, Supplementary Data 1). Using label-free quantification combined with data-independent acquisition, we identified 78 proteins as potential interactors of E2-liganded, activated ERα exceeding the statistical significance threshold (Log_2(Fold Change) >0.5, p-value < 0.05). Notably, 11 transcription factors (TF) were enriched among all significant hits. Many of those, such as *MYC* and *FOS*, are well studied proto-oncogenes involved in transcriptional co-activation with E2-liganded ERα to promote cell growth and proliferation. When comparing the enriched proteins with the data from 11 *ESR1*+ invasive breast cancer models in the Cancer Dependency Map project (DepMap Public 25Q2)[34,35], significantly more of the E2-enriched proteins were identified as common essential, suggesting their functional relevance (Supplementary Fig. 3a). By contrast, global proteomics in E2-treated MCF7 cells revealed upregulation of only 6% of these enriched proteins, indicating that the observed μMap enrichment results from labeling of neighboring interactors rather than merely increased protein abundance (Fig. 1g, I, Supplementary Data 4). Additionally, we benchmarked our platform against co-immunoprecipitation mass spectrometry (co-IP MS) in the native MCF7 nuclear fraction (Fig. 1h, Supplementary Data 3). Several proteins—including the TFs *MYC, FOS, RET, MXD1, ELF3, CCND1*, and *TIPARP*—were detected in both experiments (Fig. 1i). However, these overlapping proteins are lower in ranking among the 139 significant hits identified in the nuclear IP-MS dataset (Log_2(Fold Change) >1, p-value < 0.05). Even under more stringent selection criteria, co-IP MS produces a large number of hits, complicating efforts to deconvolute true ERα interactors. By contrast, our highly sensitive μMap platform provides an orthogonal technology for capturing the nearest interactors of ERα, which are often difficult to detect with standard co-IP-based strategies. The successful capture of known and essential E2-induced ERα interactors through N-terminal Ir-conjugation underscores the robustness and reliability of this approach for studying the ERα interactome.

Fulvestrant induces ERα's interaction with cell cycle regulators

Next, we sought to apply the established μMap platform to interrogate the ERα interactome under Fulv treatment. Comparing interactors induced by the natural ligand E2 and those induced by the antagonist Fulv allowed for the identification of gain-of-function (enriched with Fulv) and loss-of-function (enriched with E2) interactors (Fig. 2a).

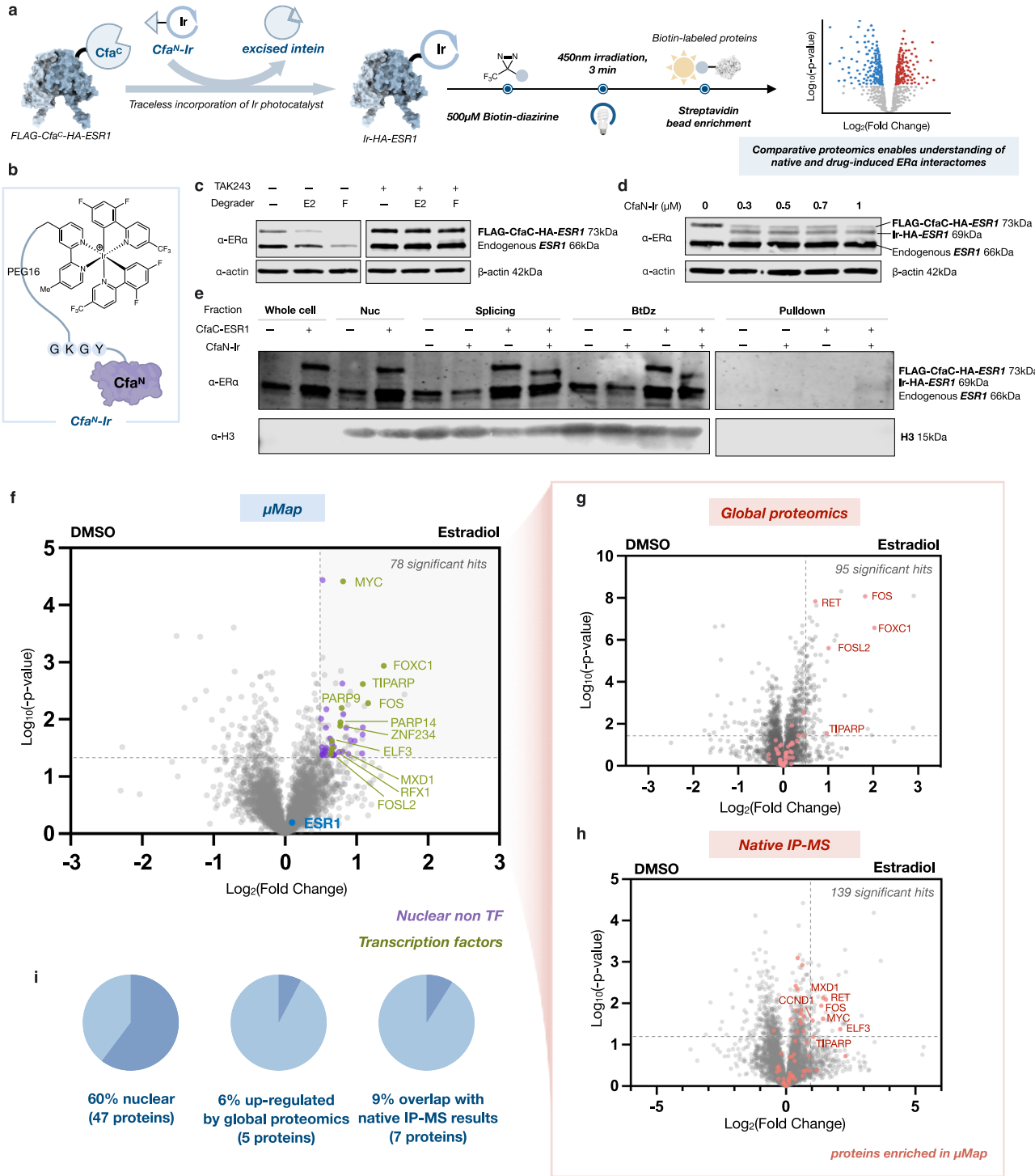

Interestingly, the TFs *MYC, FOS, TIPARP, FOXC1, ELF3*, and *MXD1*—previously identified as activated ERα interactors—are again enriched with E2 treatment (Fig. 2b, Supplementary Data 1). The absence of these E2-associated oncogenic TFs under Fulv treatment suggests their displacement from ERα, resulting in repression of proliferative transcriptional signals. In contrast, under Fulv treatment we identified a number of gain-of-function interactors associated with cell cycle regulation (Fig. 2b). Gene ontology (GO) analysis of Fulv-specific proteins (Supplementary Fig. 2d) revealed cell cycle regulators associated with growth arrest, including CDK4/6 inhibition, cellular senescence, G1 DNA damage checkpoint, and p53 signaling (Fig. 2c). Many of these hits are not significantly enriched through global proteomics, suggesting that the labeling is interaction-dependent (Fig. 2d, Supplementary Data 4). Nuclear IP-MS analysis also shares some commonality in the Fulv-specific interactors, serving as an orthogonal platform for capturing ERα stable complexes (Supplementary Data 3).

Additionally, core PML NB proteins were found to be enriched upon Fulv treatment[36–39] (Fig. 2b). PML NBs are membraneless nuclear condensates that regulate important cellular processes, such as DNA damage sensing and repair, apoptosis, and cellular senescence. They are assembled through the SUMO-interacting motif (SIM) to recruit SUMOylated proteins and interact dynamically with chromatin[40]. Based on GO analysis[41] and our evaluation of the proteins enriched in Fulv-treated photolabeling samples, we hypothesize that ERα is

Fig. 1 | Split-intein based μMap captures native ERα interactome. a μMap workflow for capturing ERα interactome in isolated nucleus. C-terminus of split intein Cfa (Cfa^C) is genetically incorporated into the N-terminus of ERα, allowing traceless incorporation of Ir photocatalyst via the addition of N-terminus of split intein Cfa conjugated to Ir (Cfa^N-Ir). The catalyst is activated with 450 nm blue LED for the local activation of biotin-diazirine warhead through Dexter energy transfer. Graphics used here were *created in BioRender. Dong, Z. (2026)* https://BioRender.com/81zwdh2. **b** Structure of Cfa^N-Ir. Ir is chemically conjugated to PEG16 and short peptide linker GKGY through strain-promoted DBCO-azide cycloaddition and amide coupling via lysine side chain amine and N-hydroxysuccinimide (NHS) ester, respectively. The conjugation to Cfa^N is achieved through native chemical ligation. Graphics used here were *created in BioRender. Dong, Z. (2026)* https://BioRender.com/81zwdh2. **c** Western blot analysis of MCF7 FLAG-Cfa^C-HA-*ESR1* cells treated with +/− 10 μM TAK-243 for 1 h prior to co-treatment with 100 nM of E2 or Fulv (F) or equal volume of DMSO as control for 4 h. Similar results were obtained in 3 independent experiments. **d** Western blot analysis of Ir incorporation onto ERα under 1 h, 37 °C end-to-end rotation of isolated nucleus of MCF7 FLAG-Cfa^C-HA-*ESR1* cells with various concentration of Cfa^N-Ir. Similar results were obtained in 3 independent experiments. **e** Western blot analysis of labeling efficiency of the splicing product Ir-HA-*ESR1*. MCF7 WT cells were used for no construct control. Fractions were preserved along the process: 'Nuc' = isolated nucleus, 'Splicing' = after 1 h 0.3 μM Cfa^N-Ir incubation, 'BtDz' = after 450 nm irradiation with biotin-diazirine, and 'Pulldown' = after streptavidin pulldown. Similar results were obtained in 3 independent experiments. **f** Volcano plot showing label-free comparative proteomics μMap upon pre-treatment of 10 μM TAK-243 for 1 h followed by the co-treatment with 100 nM E2 or DMSO as control ($n = 3$ biological replicates per condition). Among all E2-enriched proteins, transcription factors are highlighted in green, and other nuclear proteins are highlighted in purple. Global proteomics (**g**) on isolated nucleus and nuclear IP-MS (**h**) was performed with MCF7 WT cells under the same conditions. Proteins enriched were determined using two-sided Student's *t* test with cutoffs noted as dotted lines. All E2-enriched proteins from μMap above cutoff are shown as pink dots in global proteomics and nuclear IP-MS. **i** Percentage of nuclear proteins and overlaps between μMap hits and global proteomics or nuclear IP-MS among all μMap hits. Source data are provided as a Source Data file.

sequestered into PML NBs only when bound to Fulv. Further evidence came from comparing global proteomics on MCF7 WT cells treated with Fulv or DMSO. GO anaylsis[41] of those enriched hits suggests upregulation of chromatin remodeling, DNA repair, and interestingly, SUMO E3 ligase/SUMOylate target protein pathways (Supplementary Fig. 2c, Supplementary Data 5). The upregulation of such pathways is consistent with the assembly and roles of PML NB, supporting the hypothesis that Fulv-bound ERα is translocated to PML NBs.

Fulv leads to cellular senescence

The enrichment of numerous cell cycle regulators motivated us to explore the effect of Fulv on cellular growth arrest. MCF7 WT cells were treated with 1 μM E2 or Fulv for 24 or 48 h, followed by incubation in media to reach a total incubation of 8 days for senescence induction. Cell cycle analysis suggests significant reduction of cells in the G2/M phase for both Fulv treatment conditions (Fig. 3a, b). Measurement of Ki-67, a nuclear proliferation marker, also showed strong decrease of the signals in Fulv-treated cells, indicating growth arrest (Fig. 3c). To further validate whether these phenotypes indeed reflect cellular senescence, we stained for senescence-associated β-galactosidase (SA-β-gal) (Fig. 3d). Fulv triggered strong SA-β-gal expression, based on staining, compared to the proliferative conditions treated with E2 or DMSO control, confirming its ability to induce senescence.

To explore the relationship between PML NB formation and cellular senescence, we measured the phosphorylation level of protein Rb. The hypophosphorylated Rb is sequestered to PML NBs and signals for senescence through E2F recruitment[42], where phosphorylation is achieved through the cell cycle progression signal CDK4/6[43]. In E2-treated samples, we observed strong phosphorylation at S780 and S807/811, and the signal increased with extended treatment time. On the other hand, Fulv induced hypophosphorylation at those sites, as seen in the senescent positive control induced by etoposide (Ep) (Fig. 3e). The onset of cellular senescence and Rb hypophosphorylation provide functional evidence on the role of PML NBs in Fulv treatment. Furthermore, Fulv-induced Rb hypophosphorylation suggests an explanation for the synergistic effects observed with Fulv and CDK4/6 inhibitor combination therapies used in therapies[44].

SERD-bound ERα localizes to PML NBs

To validate ERα's engagement with PML NBs upon Fulv treatment, we sought to first understand the protein-protein interaction (PPI) between ERα and PML protein using co-immunoprecipitation (co-IP). While PML I isoform was the most abundant PML isoform in total lysate, PML IV—the main isoform involved in forming PML NBs—was strongly pulled down in the presence of HA-ESR1 and Fulv compared with unliganded ERα (Fig. 4a). While PML protein was not a significant interactor identified from μMap, we hypothesized that this interaction could be bridged by chromatin remodeler proteins ATRX (Fig. 2c) and DAXX (Fig. 4b), both considered to be core PML NB components and identified through μMap and nuclear IP-MS, respectively. These two proteins often complex together and localize to PML NBs to regulate gene expression, DNA damage, and other cellular processes.

Co-localization of Fulv-liganded ERα with PML was confirmed using stimulated-emission depletion (STED) super-resolution microscopy, where Fulv treatment led to significant overlap of the signals within fine puncta in the nucleus of MCF7 and T47D cells. No co-localization between ERα and PML was found under DMSO or E2 conditions (Fig. 4c, Supplementary Fig. 5b). To distinguish whether the interaction of ERα is specific to PML itself or if ERα is recruited to the PML NB structure, we examined the co-localization of ERα with ATRX, which localizes to PML NBs (Supplementary Figs.4a, 5a). We found that ERα puncta co-localize with ATRX under Fulv treatment, but not under DMSO or E2 treatments, suggesting that ERα is translocated into ATRX-containing PML NBs (Fig. 4d, Supplementary Fig. 6a). We next questioned whether the recruitment of ERα to PML NBs is specific to Fulv or is a common function among SERDs. To this end, we treated MCF7 and T47D cells with imlunestrant or elacestrant, two approved second-generation SERD drugs, and probed the co-localization of ERα and PML or ATRX. Gratifyingly, imlunestrant- and elacestrant-treated cells showed ERα localization patterns similar to those observed with Fulv. Together, these data suggest that SERD-bound ERα is translocated into ATRX-containing PML NBs.

SERD-induced translocation of ERα to PML NB affects ERα mobility and leads to cell death

In addition to promoting ERα degradation, SERDs lead to ERα immobilization[16]. Having demonstrated that SERD treatment leads to ERα sequestration into PML NBs, we questioned whether the observed immobilization arises from engagement with a nuclear condensate. To this end, fluorescence recovery after photobleaching (FRAP) was used to measure ERα mobility upon Fulv treatment in conjunction with ATRX or DAXX siRNA knockdown (Supplementary Data 6). The 60 s relative recovery of eGFP-ERα fluorescence compared to its signal immediately after the photobleaching event was calculated for each condition. Consistent with previous reports, treatment with Fulv showed little recovery of the eGFP-ERα signal (Supplementary Fig. 7c). Reduced ATRX or DAXX expression reversed Fulv-induced ERα immobilization in MCF7 and T47D cells. Treatment with ML792, a SUMO-activating enzyme (SAE) inhibitor that disrupts PML NB formation (Supplementary Fig. 7d), also rescues the ERα immobilization caused by Fulv (Fig. 5a). Imlunestrant and elacestrant-treated cells similarly induced ERα immobilization, which was reversed upon siRNA

https://doi.org/10.1038/s41467-026-77034-w

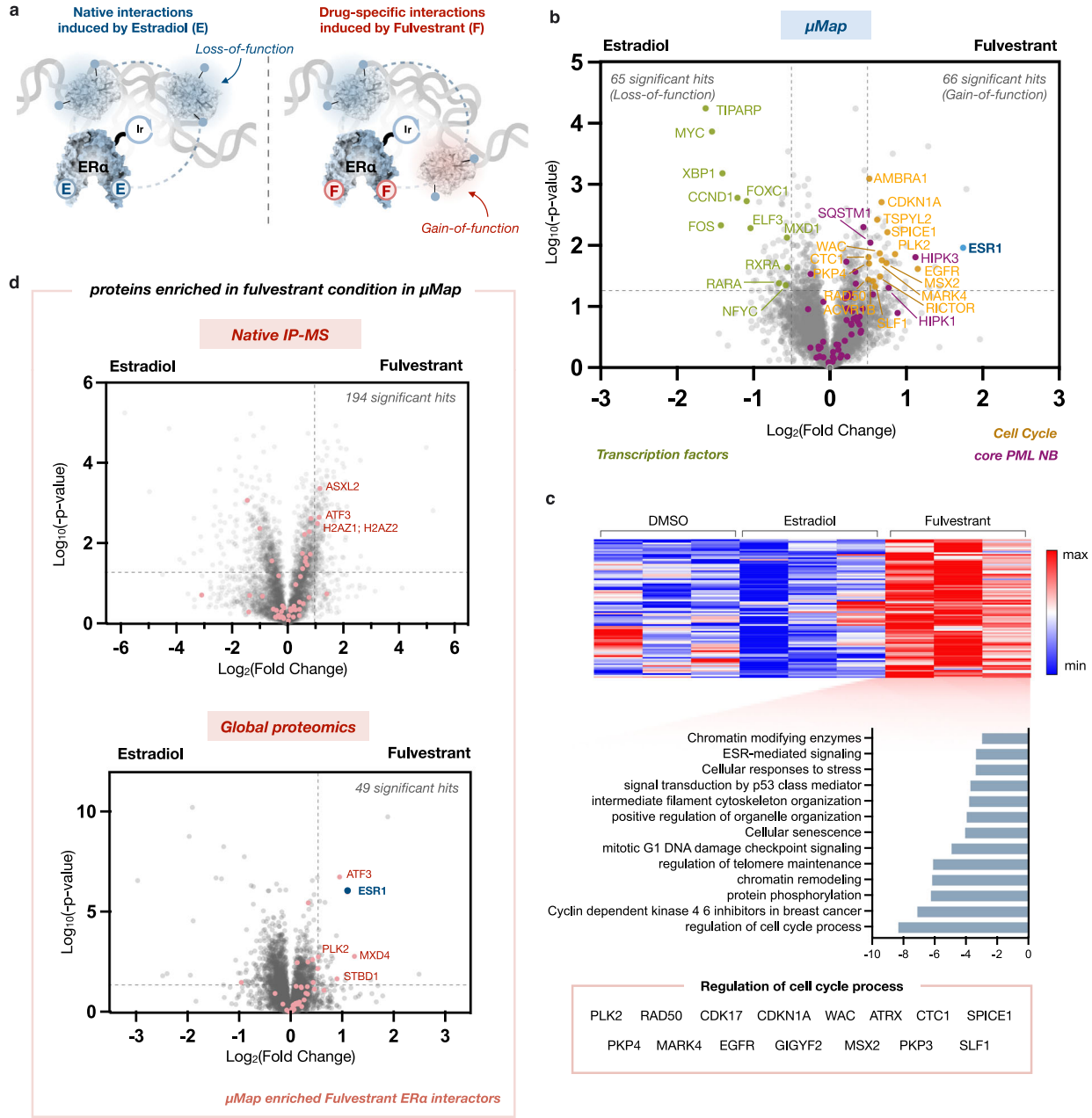

Fig. 2 | Fulvestrant-perturbed ERα interactome reveals ERα association with cell cycle regulators and core PML NB proteins. a Scheme showing μMap comparative proteomics of Fulv vs E2 treatments uncovering loss-of-function and gain-of-function ERα interactors. Graphics used here were *created in BioRender. Dong, Z. (2026)* https://BioRender.com/81zwdh2. **b** Volcano plot showing label-free ERα μMap upon pre-treatment of 10 μM TAK-243 for 1 h followed by co-treatment with 100 nM Fulv or E2 for 4 h ($n = 3$ biological replicates per condition). Proteins enriched were determined using two-sided Student's *t* test with cutoffs noted as dotted lines. Among all E2-enriched proteins, transcription factors are highlighted in green. Among all Fulv-enriched proteins, cell cycle regulators are highlighted in yellow. Core PML NB proteins among all identified proteins are highlighted in purple. **c** Gene ontology (GO) analysis of all fulvestrant gain-of-function ERα interactors. Proteins in top category "regulation of cell cycle process" are listed. **d** Volcano plot showing global proteomics on isolated nucleus and nuclear IP-MS of MCF7 WT cells upon pre-treatment of 10 μM TAK-243 for 1 h followed by co-treatment with 100 nM Fulv or E2 for 4 h ($n = 3$ biological replicates per condition). Proteins enriched were determined using two-sided Student's *t* test with cutoffs noted as dotted lines. All fulvestrant gain-of-function ERα interactors (listed in Fig. 2c) are shown as pink dots in global proteomics and nuclear IP-MS. Source data are provided as a Source Data file.

and ML792 treatment (Supplementary Fig. 6b). These results indicate that PML NBs and the bridging proteins ATRX and DAXX are responsible for SERD-mediated ERα immobility.

We further examined the impact of these perturbations on cell viability. In MCF7 cells, both knockdown of DAXX and treatment with ML792 rescued Fulv-mediated cell death. In T47D cells, while knockdown of DAXX or ATRX alone did not reverse Fulv-mediated cell death, SUMOylation inhibition using ML792 showed significant rescue of Fulv-mediated cell death (Fig. 5b). We reasoned that the different responses between the two cell lines to DAXX knockdown could arise from differences in the expression of apoptotic and proliferative proteins, including p53 and the progesterone receptor[45,46]. To establish the generality of the effects of PML NB disruption, we similarly co-treated the cells with elacestrant and imlunestrant. Inhibition of SUMOylation consistently reversed SERD-mediated cell death (Supplementary Fig. 6c). ML792 alone induced modest cell cycle arrest;

https://doi.org/10.1038/s41467-026-77034-w

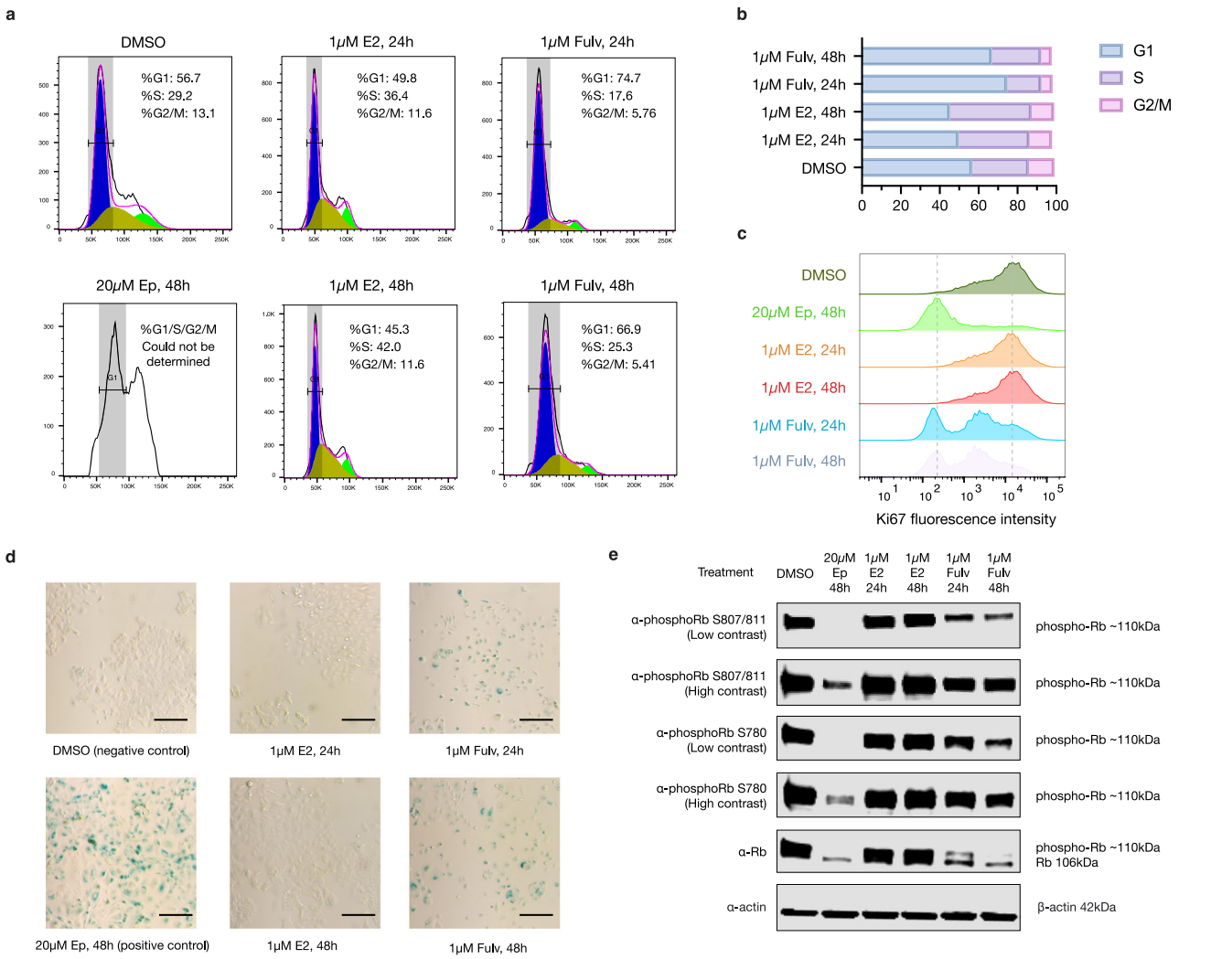

Fig. 3 | Fulvestrant induces senescence in MCF7 cells. a–**e** MCF7 WT cells treated with noted conditions and cultured continuously in DMEM with phenol red supplemented with 10% FBS and 1% penicillin-streptomycin to reach 8 days in total for senescence induction. **a**, **b** Cell cycle was determined through DAPI staining and flow cytometry. Dean-Jett-Fox model with synchronized peak and G2 peak = G1x2 was used. **c** Ki-67 measurement through flow cytometry. **d** Beta-galactosidase staining. Scale bar = 0.2 mm. **e** Western blot analysis of Rb and phospho-Rb levels. For (**d**) and (**e**), similar results were obtained in 3 independent experiments. Source data are provided as a Source Data file.

however, in combination with Fulv, it partially mitigated Fulv-induced growth inhibition (Fig. 5b). These findings indicate that Fulv-induced ERα immobility, cell death, and growth arrest are dependent on SUMOylation and the formation of PML NBs. Given the role of PML NBs in senescence and apoptosis, disrupting the sequestration of Fulv-liganded ERα into the membraneless organelle may alter downstream signaling pathways and enhance cell viability.

After establishing the functional relevance of the sequestration of ERα into PML NBs, we then sought to understand the mechanism of the interaction by examining the role of each ERα domain. We investigated the co-localization of ERα with PML NBs using STED microscopy in U2OS cells transfected with truncated HA-tagged ERα constructs. U2OS cells express low endogenous levels of ERα, enabling selective visualization of transfected constructs. Under Fulv treatment, full-length HA-*ESR1*, HA-*ESR1*ΔA/B, HA-*ESR1*ΔC, and HA-*ESR1*ΔF retained engagement with PML and ATRX in U2OS cells. However, deletion of domain D abrogated ERα's interaction with PML and ATRX, while deletion of domain E disrupted punctate formation of ERα under Fulv treatment (Fig. 5d, Supplementary Fig. 8a, b). Domain E is the ligand binding domain of ERα[47]. Thus, deletion of domain E disables Fulv binding to ERα, resulting in the diffuse distribution of ERα in the nucleus. Domain D is a short hinge region that connects the DNA-binding domain of ERα with the ligand-binding domain. Importantly, domain D has been found to contain multiple SUMOylation sites[44]. The disruption of ERα-PML NB interaction upon deletion of the SUMOylation-containing domain D is consistent with our previous results revealing the importance of SUMOylation on Fulv-induced effects. Together, these data suggest that SUMOylation drives the interaction of ERα with PML NBs under Fulv treatment and contributes to SERD function.

Fulv induces redistribution of ERα-DNA binding

Since PML NBs are known to associate with chromatin and alter the epigenetic landscape, we next investigated the relationship between ERα and DNA under both E2 activation and Fulv antagonism. To first assess ERα's engagement with chromatin, MCF7 cells treated with DMSO, E2, or Fulv were fractionated into cytosolic, nuclear soluble, and chromatin nuclear insoluble fractions. Western blot analysis suggests that, although overall levels of ERα decreased upon Fulv treatment, the remaining Fulv-bound ERα was preferentially enriched in the chromatin fraction, in contrast to E2-bound ERα, which was more abundant in the nuclear soluble fraction (Fig. 6a). This trend was

https://doi.org/10.1038/s41467-026-77034-w

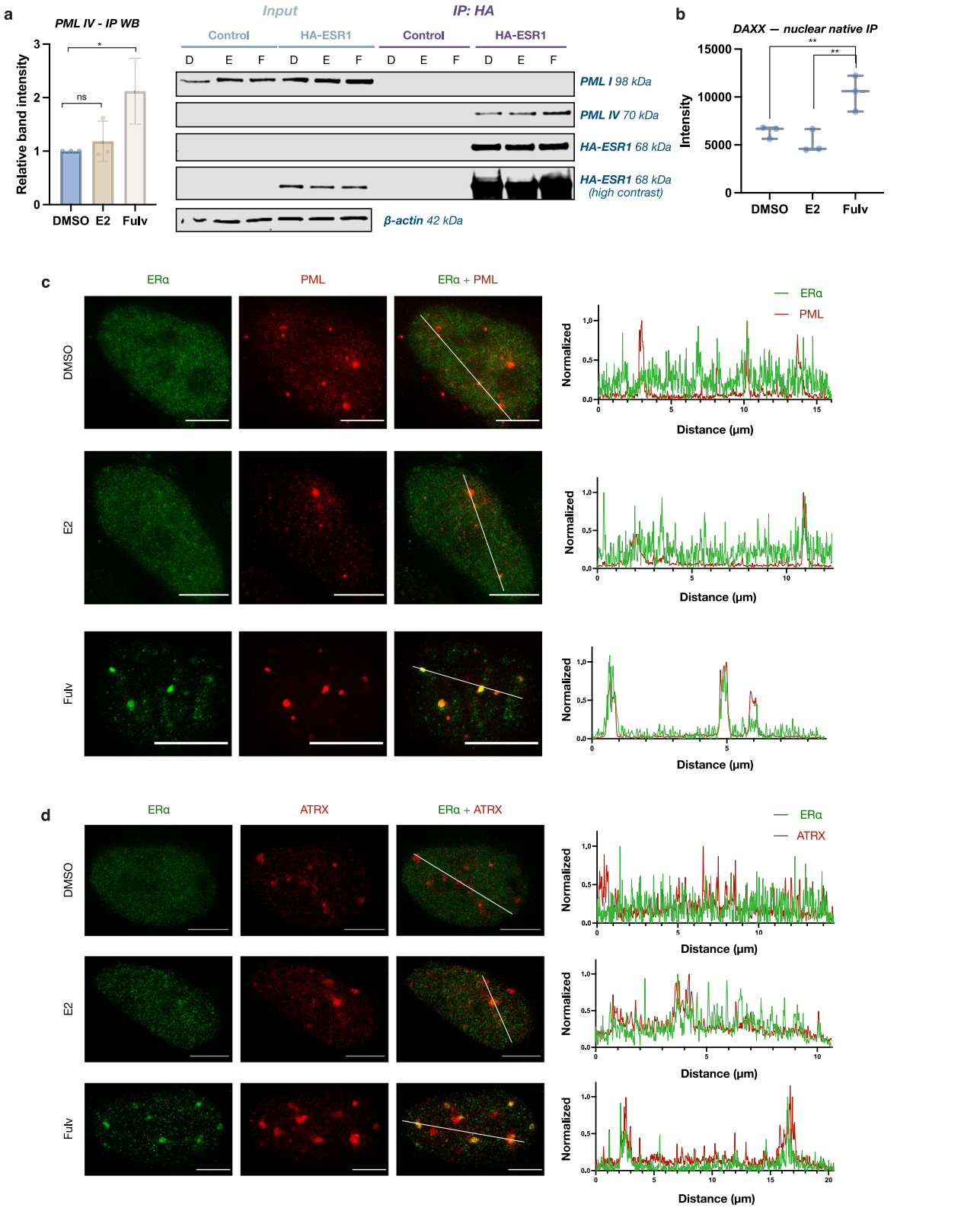

Fig. 4 | Fulv-liganded ERα is translocated into PML NB. a Co-immunoprecipitation of HA-tag in HEK 293T cells transfected with HA-*ESR1* or empty vector as control. Relative band intensity was calculated after normalizing with input PML IV level, shown as means +/− SD. DMSO/100 nM E2/100 nM Fulv was spiked into the lysate to induce protein-protein interactions. Statistical significance was calculated from 3 biological replicates. *$p = 0.0347$ (one-way ANOVA test). **b** Intensity of DAXX in native IP-MS against ERα in MCF7 WT cells treated with 100 nM of estradiol or fulvestrant or equal volume of DMSO. Data are presented as mean +/− SD, with $n = 3$ (biological replicates), **$p = 0.0072$ (one-way ANOVA test). **c**, **d** Super-resolution microscopy using Stimulated Emission Depletion microscopy (STED) of ERα and ATRX or PML under 100 nM estradiol or fulvestrant or equal volume of DMSO for 4 h. Scale bar = 5μm. Line profile plots depict normalized fluorescence intensity for ERα (green) and ATRX or PML (red) along the white line drawn across the nuclei marked on the left of each line profile plot. For (**c**, **d**), similar results were obtained in 3 independent experiments. Source data are provided as a Source Data file.

https://doi.org/10.1038/s41467-026-77034-w

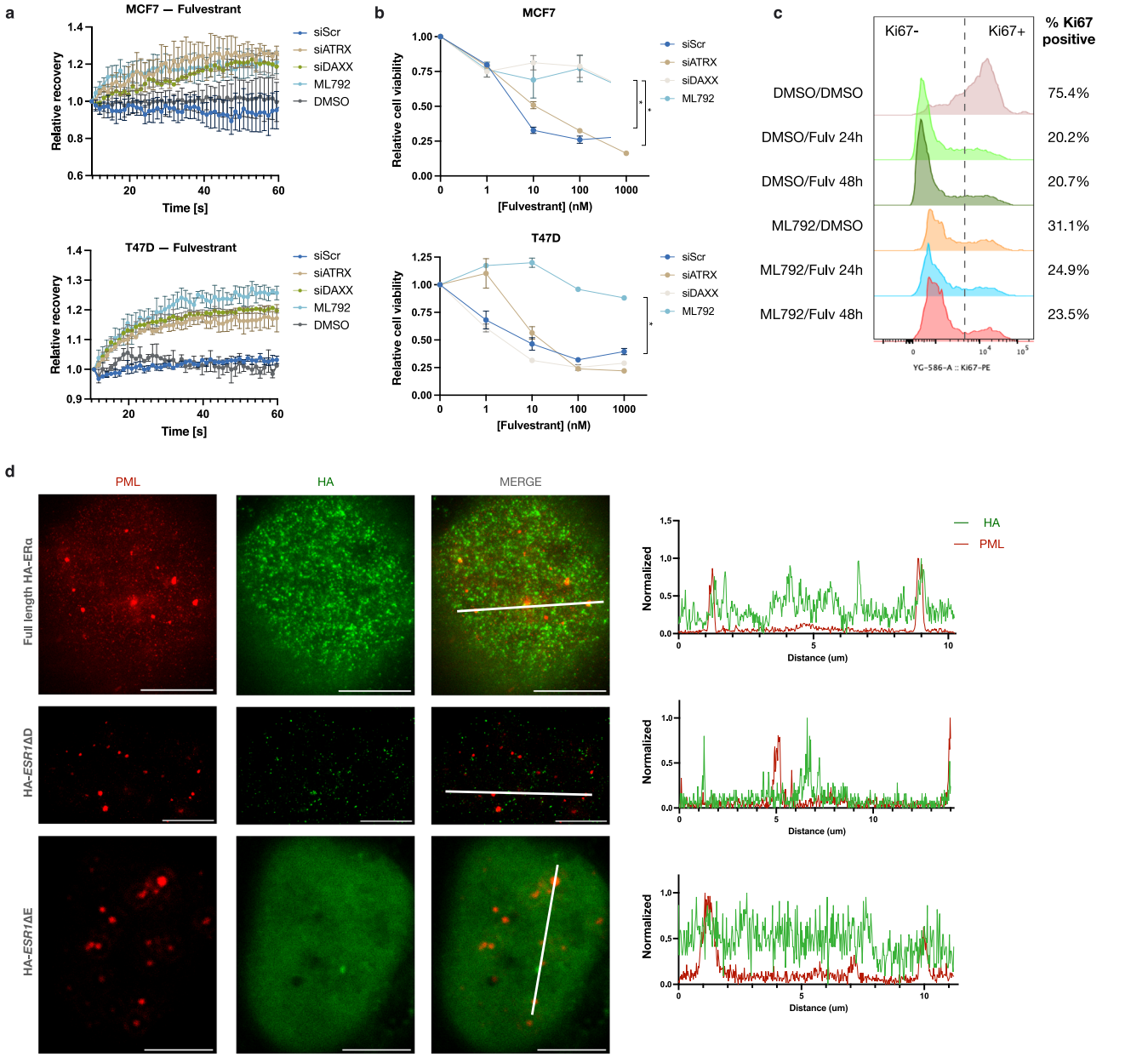

Fig. 5 | ATRX, DAXX, and SUMOylation are important for Fulv-induced effects and the translocation of ERα into PML NB. a Fluorescence Recovery After Photobleaching (FRAP) analysis of MCF7 and T47D cells transfected with eGFP-*ESR1* along with co-transfection of the corresponding siRNAs or co-treatment of 10 μM ML792 while being treated with 100 nM Fulv for 4 h. Each condition contains 3 biological replicates. Relative recovery was calculated based on the initial bleached signal and shown as mean +/− SEM. **b** Relative cell viability measured in MCF7 and T47D cells transfected with the corresponding siRNAs or treated with 10 μM ML792 along with 100 nM Fulv at different concentrations for 8 days. Cell viability was normalized using DMSO treated cells for each corresponding group and shown as mean +/− SEM. Each condition contains 3 biological replicates. *$p < 0.05$ (one-way ANOVA test). **c** Ki-67 measurement of cells pretreated with 1 h of 10 μM ML792 or DMSO prior to the co-treatment of 100 nM fulvestrant for noted durations with an additional culturing for 6 days for senescence induction. **d** STED images in U2OS cells staining for PML (red) and HA (green) after treating cells with 100 nM Fulv for 4 h and transfecting with full length HA-*ESR1*, HA-*ESR1*ΔD or HA-*ESR1*ΔE. Line profile plots depict normalized fluorescence intensity for HA (green) and PML (red) along the white line drawn across the nuclei marked on the left of each line profile plot. Scale bar = 5 μm. Similar results were obtained in 3 independent experiments. Source data are provided as a Source Data file.

amplified upon addition of the UAE inhibitor, TAK-243. While it is expected for E2 to initiate engagement of ERα with chromatin for transcription upregulation, the even stronger association observed between Fulv-liganded ERα and chromatin could potentially be explained by sequestration of ERα into chromatin-bound PML NBs.

To interrogate the ERα-DNA interactions at specific loci, we conducted Cleavage Under Targets and Release Under Nuclease (CUT&RUN), as it is more reliable for the study of large, insoluble protein complexes such as PML NBs[48] (Supplementary Data 7). CUT&RUN peak numbers indicate that ERα is associated with chromatin to a similar extent when bound to either E2 or Fulv (Fig. 6b). However, Fulv binding led to increased interactions in promoter regions and fewer interactions in intron and distal intergenic regions (Fig. 6c). In DMSO, E2, and Fulv-treated cells, ERα binds the estrogen-responsive element (ERE) motif (GGTCANNNTGACC) to different extents (Supplementary Fig. 9e). Position weight matrix (PWM) log-odds scores were used to evaluate peaks containing at least one significant ERE match. While the DMSO control exhibited a broad

https://doi.org/10.1038/s41467-026-77034-w

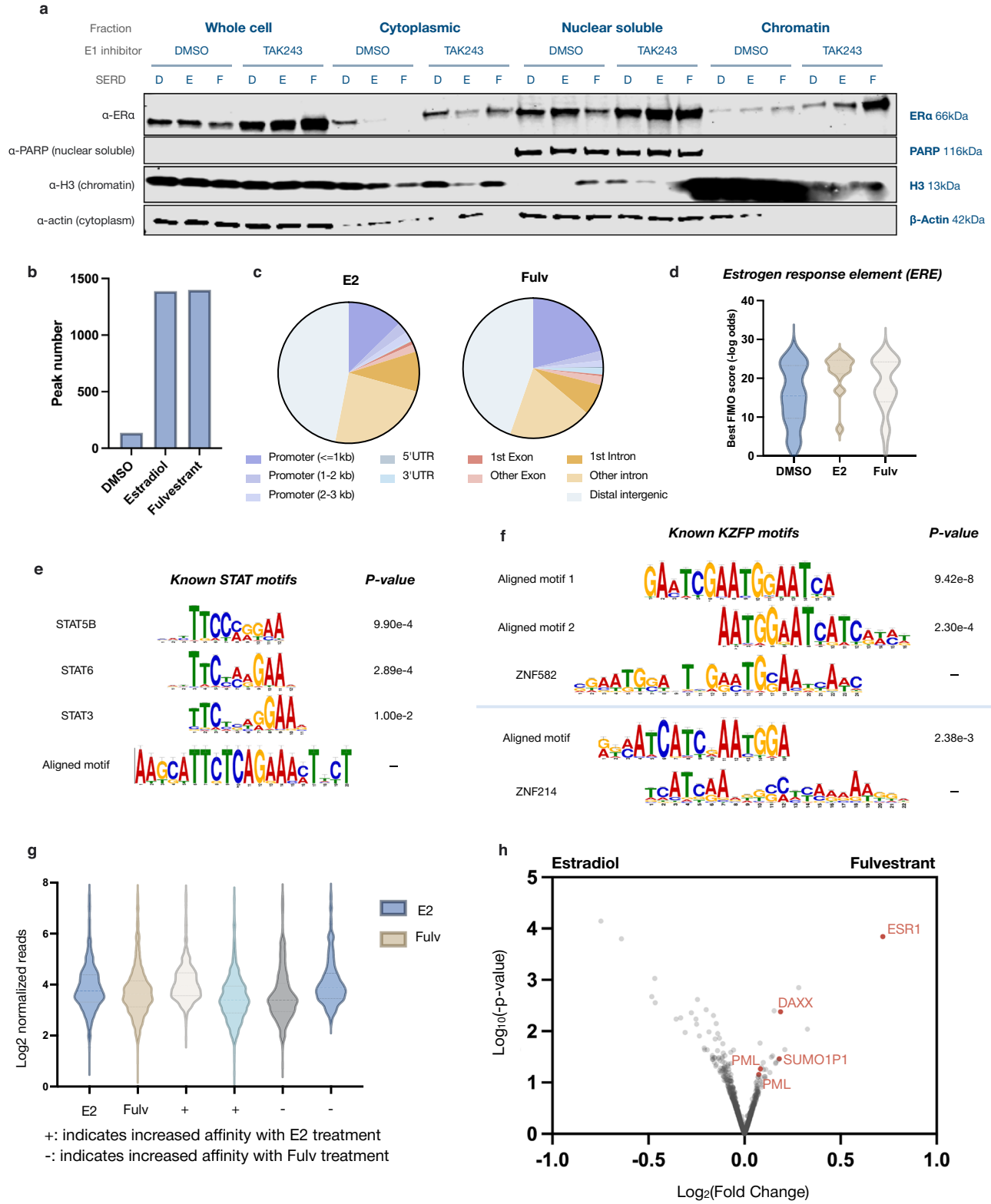

Fig. 6 | Fulv induces redistribution of ERα-DNA binding. a Fractionation analysis of ERα in MCF7 WT cells pre-treated with 10 μM TAK-243 or DMSO prior to co-treatment with 100 nM E2 or Fulv or DMSO for 4 h. Similar results were obtained in 3 independent experiments. **b**–**i** ERα CUT&RUN experiment with MCF7 cells treated with 100 nM E2 or Fulv or DMSO for 45 min. Two biological replicates were performed. **b** Total peak counts in each condition identified using MACS2 Version 2.2.7.1. **c** Regions of DNA where ERα binds to were identified using ChIPseeker Version 1.28.3. **d** Distribution of position weight matrix (PWM) scores of ERE in DMSO, E2, or Fulv treated samples calculated using FIMO (MEME-Suite Version 5.5.5). **e** STAT protein binding motifs aligned to ERα-DNA binding motifs identified in E2 treated cells. **f** KZFP protein binding motifs aligned to ERα-DNA binding motifs identified in Fulv treated cells. **g** Distribution of ERα-DNA occupancy under E2 and Fulv treatment as shown using the $\log_2$-normalized read counts. Read counts were normalized using DiffBind Version 3.12.0. **h** Differential binding occupancy between E2 and Fulv treated ERα calculated using DiffBind Version 3.12.0. *P* values were calculated using a negative binomial GLM and Wald test. For (**e**, **f**), *p* values were computed using Tomtom (MEME Suite), from an empirical null distribution of column-similarity scores (Euclidean distance) by sampling target motif columns. Source data are provided as a Source Data file.

distribution of PWM scores, E2 treatment resulted in a marked enrichment of high-affinity binding. Fulv-treated ERα maintained a population of high-scoring motifs but displayed a more dispersed distribution than the E2 condition, suggesting a partial capacity to occupy ERE-containing sites (Fig. 6d). By aligning the top motifs identified from MEME-ChIP with known DNA motifs using Tomtom, we identified multiple STAT TF binding motifs associated with E2 treatment (Fig. 6e, Supplementary Data 4). Notably, previous reports have shown that signal transducer and activator of transcription (STAT) 5b association with ERα can potentiate STAT5b-responsive promoter[49]. STAT3 has also been found to co-occupy STAT3 motifs with ERα in breast cancer contexts[50]. In contrast, under Fulv treatment, two major DNA binding motifs align well with zinc-finger protein (ZNF) 582 and ZNF214 motifs (Fig. 5g, Supplementary Data 4). These motifs belong to the family of Kruppel-associated box (KRAB)-containing zinc finger proteins (KZFP), which are known to have PML protein association[51]. This interaction between ERα and KZFP motifs suggests that ERα-chromatin binding sites are altered due to the change in its nuclear localization. DiffBind analysis revealed a comparable level of overall DNA occupancy between E2 and Fulv-bound ERα. However, transcription factor occupancy between the two groups showed directional differences. There is a clear subset of sites where binding is significantly recruited to E2-bound ERα or Fulv-bound ERα (Fig. 6g). Interestingly, when comparing the differential chromatin binding of ERα between E2- and Fulv-treated cells, Fulv treatment increased ERα occupancy to the *ESR1* gene. In addition, Fulv-bound ERα binds to sites in *PML*, *DAXX*, and *SUMO1P1* genes more strongly than does E2-bound ERα (Supplementary Fig. 9c, d). While TF is known to bind to exons[52] and regulate transcription[53], the implication in chromatin remodeling and the interaction with nuclear condensates are relatively underexplored. Overall, our results indicate that Fulv induces epigenetic changes globally and reshapes the ERα-chromatin association landscape.

Discussion

Since its discovery in the early 1990s, Fulv has been widely regarded as an effective breast cancer therapy that antagonizes ERα through receptor depletion—an understanding reflected in its designation as a selective estrogen receptor degrader (SERD). However, several in vitro, pre-clinical, and clinical studies have shown that some of the potent ERα degraders, including amcenestrant, GDC-0810, and AZD-9496[11–13,15], do not surpass fulvestrant in reducing tumor size and preventing breast cancer progression. Recent work has shed light on fulvestrant's ability to mediate ERα immobilization, a mechanism whose importance has been obscured by the emphasis on degradation in explaining SERDs' anti-tumor effects[16]. As efforts to develop next-generation SERDs and combination therapies continue, defining the molecular basis of fulvestrant action, particularly the protein-protein interactions it governs, remains critical.

In this study, we built upon our previously reported split intein-based μMap photo-proximity labeling platform[32] to achieve precise labeling of the nearest ERα interactors induced by both natural and therapeutically-relevant ligands. The traceless incorporation of the Ir photocatalyst at the N-terminus minimally perturbs ERα native function and further reduces the labeling radius by eliminating the need for antibody-directed Ir photocatalyst localization. Our μMap interactome not only allows for the identification of known E2-responsive ERα TF interactors, such as MYC and FOS, but also suggests their displacement during Fulv treatment. Additionally, cell cycle regulator proteins are identified as Fulv-specific ERα interactors, implicating them in Fulv-induced cellular senescence.

Here, we demonstrate that Fulv treatment induces a previously unknown relocalization of the ERα nanoenvironment to PML NBs, contributing to ERα immobility, altered chromatin binding patterns, cellular senescence, and diminished survival. Second-generation SERDs, elacestrant and imlunestrant, similarly induced ERα-PML NB interactions. We found that the PML NB proteins ATRX and DAXX play important roles in engaging SERD-bound ERα in PML NBs. In addition, global reduction of cellular SUMOylation and ablation of ERα SUMOylation sites eliminated ERα engagement with PML NBs and reversed SERD-induced functional effects. Previous studies have shown that fulvestrant and elacestrant induces SUMOylation of ERα[54]. As recruitment of PML NB proteins is SUMO-dependent, our findings suggest that SERD-bound ERα is recruited to ATRX- and DAXX-containing PML NBs in a SUMO-dependent fashion. The importance of ERα-PML NB interactions under SERD treatment offers an explanation for the correlation between ERα mobility and the anti-proliferative functions of SERDs[16]. These findings may also provide a mechanistic basis for recent reports identifying RNF111 as the E3 ubiquitin ligase mediating Fulv-induced ERα degradation. Notably, RNF111 is a SUMOylation-recognizing E3 ubiquitin ligase that localizes to the PML NB[55].

Interestingly, hypophosphorylated Rb, a known PML NB component, is phosphorylated by the G1/S phase checkpoint CDK4/6 in response to CCND1 signal[43]. Our proximity labeling data suggests that the translocation of Fulv-liganded ERα could abrogate ERα engagement with CCND1 and promote Rb hypophosphorylation. In combination with Fulv, CDK4/6 inhibitors palbociclib, ribociclib, and abemaciclib have each shown significant benefits in HR+/HER2 breast cancer patients[56]. These μMap-based studies offer an additional perspective on the mechanistic basis of this therapeutic synergy, potentially through enhanced growth arrest.

PML NBs are increasingly recognized as the hubs for dynamic PPIs, post-translational modifications, gene regulations, and more. However, a better understanding of their heterogeneity and mechanistic role in chromatin regulation is required for their development as a therapeutic target or relevant biomarkers in breast cancer. Additionally, as this study was focused on a cellular ER+ breast cancer model using MCF7 and T47D cells, future experiments in ESR1 mutants, Fulv-resistant cell lines, animal models, and other ER+ cancer types could enhance our understanding of Fulv's anti-tumor mechanism and inform the development of next-generation SERDs. Future studies may further expand the detectable interactome by tuning the μMap labeling radius[33].

In conclusion, we leverage the ERα μMap platform with orthogonal methods to reveal functionally relevant protein-protein interactions, with implications for the development of next-generation ERα-targeting therapies. More broadly, the precision and sensitivity of μMap render this platform suitable for the mechanistic study of other nuclear condensates and proteins engaged in complex protein-chromatin networks.

Methods

Small molecules and antibodies

TAK-243 (HY-100487), etoposide (HY-13629), estradiol (HY-B0141), fulvestrant (HY-13636), elcestrant (HY-19822), imlunestrant (HY-145572), ML792 (HY-108702) were all purchased from MedChemExpress. Ir-DBCO, Cfa^{C}-Ir, and biotin-PEG3-diazirine probe were synthesized as previously described[32].

The following primary antibodies were used for western blotting and immunofluorescence: rabbit anti-ERα (Cell Signaling Technology, D8H8), rabbit anti-ERα (Cell Signaling Technology, D6R2W), mouse anti-ERα (Santa Cruz, sc-8002), mouse anti-β-actin (Cell Signaling Technology, 8H10D10), rabbit anti-phospho-Rb (Ser780) (Cell Signaling Technology, D59B7), rabbit anti-phospho-Rb (Ser807/811) (Cell Signaling Technology, D20B12), mouse anti-Rb (Cell Signaling Technology, 4H1), rabbit anti-PML (Invitrogen, PA5-51039), mouse anti-PML (Santa Cruz, sc-966), rabbit anti-ATRX (Invitrogen, PA5-21348), rabbit anti-HA-Tag (Cell Signaling Technology, C29F4), rabbit anti-PARP (Cell

Signaling Technology, 9542), rabbit anti-Histone H3 (Cell Signaling Technology, D1H2), rabbit anti-DAXX (Invitrogen, PA5-79137).

The following antibody-fluorophore conjugates were used for flow cytometry: mouse anti-Ki67-PE (BD Pharmingen, 556027), Annexin V-Alexa Fluor 647 (Invitrogen, A23204).

The following secondary antibodies were used for western blotting: IRDye 680RD goat anti-mouse (LI-COR, 926-68070), IRDye 680RD goat anti-rabbit (LI-COR, 926-68071), IRDye 800CW goat anti-mouse (LI-COR, 926-32210), IRDye 800CW goat anti-rabbit (LI-COR, 926-32211) and IRDye 800CW streptavidin (LI-COR, 926-32230).

The following secondary antibodies were used for immunofluorescence with confocal microscopy: Goat anti-rabbit Alexa Fluor 488 (Invitrogen, A32731), goat anti-mouse Alexa Fluor 488 (Invitrogen, A11001), goat anti-rabbit Alexa Fluor 555 (Invitrogen, A21428) and goat anti-mouse Alexa Fluor 555 (Invitrogen, A21422). The following secondary antibodies were used for immunofluorescence with STED microscopy: STAR RED goat anti-rabbit IgG (Abberior, STRED-1002-500UG), STAR ORANGE goat anti-mouse IgG (Abberior, STORANGE-1001-500UG).

Preparation of Cfa^N-Ir (Supplementary Fig. 10)

The C-terminal peptide hydrazides (1) were synthesized on a 0.05 mmol scale by standard Fmoc solid-phase peptide synthesis methods using PyAOP/DIEA activation. Before the coupling steps, Trityl-OH ChemMatrix resin was treated with 2% thionyl chloride in DCM overnight with rotation. After washing with 2× DCM and 1× with 0.5% DIEA in DCM, 5 eq. of Fmoc-hydrazide and 10 eq. of DIEA in DMF was added to the resin for 1 h with N_2 bubbling. After deprotection with 20% piperidine in DMF for 15 min, 5eq. of amino acids Fmoc-Tyr(tBu)-OH, Fmoc-Gly-OH, Fmoc-Lys(Alloc)-OH, and Fmoc-Gly-OH were sequentially coupled using PyAOP (5eq.) and DIEA (5eq) in DMF for 15 min with N_2 bubbling. Each deprotection step was followed by 3× DMF washes, and each coupling step was followed by 3× DMF and 3× DCM washes.

To conjugate the PEG16 linker (2), Alloc deprotection was performed with $Pd(PPH_3)_4$ (1eq.) and Dimethyl barbituric acid (10eq.) in DMC for 1 h with N_2 bubbling. After washing with DCM and DMF 3× each, NHS-PEG16-Azide (1eq.) was added to the resin with 1% DIEA in DMF. The reaction lasted 3 h with N_2 bubbling and was followed by washes with DMF and DCM 3× each. The resulting peptide was deprotected with 20% piperidine in DMF twice for 15 min and cleaved using TFA:TIPS:H_2O (95:2.5:2.5 v/v/v) with 1 h rotation at room temperature. The supernatant was filtered and reduced to minimal volume before the addition of 40× volume of H_2O for lyophilization.

Thioester conversion was performed first by dissolving the peptide-PEG16 in ice-cold conversion buffer (200 mM KH_2PO_4, 6 M Gdn-HCl, pH = 3). $NaNO_2$ was added to the solution to reach 100 mM, and the reaction was carried out for 20 mins at −20 °C. MESNa was then added to the mixture to reach 0.67 mM and followed by pH adjustment to pH = 7. The reaction was performed at room temperature for 20 min before diluting with 10× volume of 0.1%FA in H_2O and pH adjustment to pH = 3. The thioester peptide (3) was purified using 10-80% 0.1%FA in MeCN gradient on prep-HPLC. The correct fraction was collected and lyophilized.

Click chemistry (4) was performed by first dissolving the peptide thioester in ligation buffer (200 mM KH_2PO_4, 6 M Gdn-HCl, pH = 7) and adding 2eq. of Ir-DBCO[32]. Mix the solution well and add DMSO until the solution is clear before incubation at room temperature for 1 h. The reaction was purified using 10–80% 0.1%FA in MeCN gradient on prep-HPLC. The correct fraction was collected and lyophilized.

Final native chemical ligation was performed using CfaN-KSK-SUMO[57] with 1.5eq. of Ir-PEG16-thioesther peptide in ligation buffer with 20 mM TCEP. Add 1% TFET and carefully adjust pH to 7 before incubating at room temperature for 2 h. The product was purified using 30–70% 0.1%TFA in MeCN gradient on prep-HPLC. The correct fraction was collected and lyophilized. Protein refolding was performed by dissolving the lyophilized product in DPBS supplemented with 1 mM DTT and 6 M urea. A step-wise dialysis was performed using Slide-A-Lyzer G2 Dialysis Cassette (7k MWCO) in 4, 2, and 0 M urea in 1 mM DTT in DPBS for 2 h each, followed by an additional overnight dialysis with 0 M urea in 1 mM DTT in DPBS. 15%v/v glycerol was added at the end of the dialysis for storage. The final product was quantified and stored at −80 °C.

Plasmid generation

FLAG-Cfa^C-HA-*ESR1* and *ESR1*-HA-Cfa^N-FLAG plasmids were cloned into pCDH-UbC-MCS-EF1-Puro vector using standard restriction cloning procedures. HA-*ESR1*, HA-*ESR1*ΔA/B, HA-*ESR1*ΔC, HA-*ESR1*ΔD, HA-*ESR1*ΔE, HA-*ESR1*ΔF were cloned into pcDNA3.1(+) using standard Gibson assembly cloning procedures. All sequences are available in Supplementary Data 8.

Cell culture, lentiviral production and generation of stable cell lines

MCF7 cells were obtained from ATCC (HTB-22), and T47D cells were generously gifted by Dr. Yibing Kang at Princeton University. The FLAG-CfaC-HA-*ESR1* MCF7 stable cell line was generated by lentiviral transduction. Briefly, a FLAG-CfaC-HA-*ESR1* lentiviral expression plasmid was co-transfected with 2nd generation lentiviral packaging system (ABM) into Lenti-X 293T cells (Clonetech) using Lipofectamine 2000 (Invitrogen, 11668019). Following overnight incubation media was removed and fresh DMEM was added to Lenti-X 293T cells. Thirty-six hours later viral supernatant was collected and filtered through a 0.45 micron cellulose acetate filter. MCF7 cells were later infected with lentivirus supernatant. After 24 h, viral supernatant was removed and complete culture media was added to the cells containing 1 μg mL^{-1} puromycin. Cells were incubated for 72 h. Media was removed and fresh media containing selection antibiotic was added. Cells were passaged for an additional 11d with the selection antibiotic to select cells stably integrated with FLAG-CfaC-HA-ESR1 lentiviral expression plasmids. MCF7, U2OS, and HEK293T cells were cultured in DMEM (Gibco, 11995065) supplemented with 10% FBS (Gibco, 10437028) and 1% penicillin-streptomycin (Gibco, 15070063) at 37 °C and 5% CO_2 atmosphere in standard cell culture dishes. T47D cells were cultured in RPMI 1640 media (Gibco 11875093) supplemented with 10% FBS (Gibco, 10437028) and 1% penicillin-streptomycin (Gibco, 15070063) under the same condition. Prior to estradiol or fulvestrant treatment, cells were incubated in phenol red-free DMEM or RPMI 1640 (Gibco, 31053028 or 11835030) supplemented with 10% charcoal-stripped FBS (Gibco, 12676029), 1% penicillin-streptomycin, and 1% L-glutamine (Gibco, 25030081) at 37 °C and 5% CO_2 atmosphere in standard cell culture dishes for 3 days unless otherwise noted.

Intein trans-splicing and proximity labeling

All cells used for proximity labeling were cultured in 10 cm cell culture plates to ~7×10^6 with phenol-red free DMEM supplemented with 10% charcoal-stripped FBS, 1% penicillin-streptomycin, and 1% L-Glutamine for 3 days before treatment. Each replicate contains 2 plates of 10 cm plate worth of cells, and each arm was performed in triplicate. The cells were pretreated with 10 μM TAK-243 for 1 h before co-treating with 100 nM DMSO/estradiol/fulvestrant for 4 h. Cells were then harvested with phenol-red free TrypLE Express. The resulting cell pellets were washed with DPBS (Gibco, 14190136) twice before washing with 600 μL RSB buffer (10 mM Tris, 15 mM NaCl, 1.5 mM $MgCl_2$, Roche cOmplete EDTA-free protease inhibitors, pH 7.6) with corresponding drugs. Nucleus extraction was achieved via homogenization using Dounce homogenizer (Wheaton, 357538) for 10 strokes in 1 mL of RSB buffer noted above. The nuclear pellets were washed with 600 μL cross-linking (XL) buffer (20 mM HEPES, 1.5 mM $MgCl_2$, 150 mM KCl, Roche cOmplete EDTA-free protease inhibitors, pH 7.6) with corresponding

drugs once before incubating in 0.3 µM CfaN-Ir in 200 µL of XL buffer at 37 °C for 1 h with rotation in darkness. After splicing, the pellets were washed 3× with 400 µL XL buffer before the addition of 500 µM biotin-PEG3-diazirine in 200 µL XL buffer and 450 nm irradiation for 3 min at 100% intensity at 4 °C. The pellets were washed 2× with 400 µL XL buffer before lysed with LB3 buffer (10 mM Tris, 100 mM NaCl, 1 mM EDTA, 0.5 mM EGTA, 0.1% sodium deoxycholate, 0.5% sodium lauroyl sarcosinate, Roche cOmplete EDTA-free protease inhibitors, pH 7.5), sonicated at 35% intensity for 2 ×10 s, and centrifugation at 18,000 × *g* for 15 min at 4 °C. Supernatants were transferred into new tubes and quantified by BCA assay (Thermo Scientific, 23225).

Strepavidin enrichment for western blotting

200 µg of nuclear labeled lysate was loaded onto 20 µL of Strepavidin Mag Sephrose beads (Cytiva, 28985799) pre-washed once with 1× binding buffer (25 mM Tris, 150 mM NaCl, 0.25% v/v NP-40, pH 7.5). The lysate was incubated overnight at 4 °C with end-to-end rotation before the following washes: 2× 1% SDS in DPBS, 2× 1 M NaCl, and 2× 10% EtOH in DPBS. The resulting beads were resuspended in DPBS and transferred into a new Lo-Bind tube, pelleted and incubated with 50 µL of freshly made elution buffer (30 mM biotin, 6 M urea, 2 M thiourea, 2% SDS in DPBs and 25% 4× Laemmli with beta-mercaptoethanol (pH 11.5)). Elution happened with heating to 95 °C for 5 min with 1000 rpm shaking. Supernatant was collected and cooled prior to western blot analysis.

Strepavidin enrichment for label-free proteomics

250 µg of nuclear lysate was loaded for each replicate in the format of 0.5 mg/mL of 500 µL total in binding buffer (25 mM Tris, 150 mM NaCl, 0.25% v/v NP-40, pH 7.5). The normalized lysates were reduced using 50 µL of 100 mM dithiothreitol (DTT) at 95 °C for 5 min with shaking, capped using 37.5 µL of 200 mM iodoacetamide (IAA) by rotating in dark for 30 min at room temperature, and quenched by 100 µL of 100 mM DTT by rotating for 15 min at room temperature. The resulting lysates were loaded onto 25 µL of Strepavidin Mag Sephrose beads (Cytiva, 28985799) prewashed with 3× 500 µL of binding buffer and rotated overnight at 4 °C. The residue supernatants were removed, and the beads were washed with 3× 500 µL of 1% SDS in DPBS, 2× 500 µL of 1 M NaCl in DPBS, 1× 500 µL of 10% EtOH in DPBS, and finally 3× 500 µL of 50 mM ammonium bicarbonate in Optima water (Fisher Scientific, W64). The washed beads were transferred to a new 1.5 mL Lo-Bind Eppendorf tube using 500 µL of 50 mM ammonium bicarbonate before the removal of solution and resuspended in 30 µL of 50 mM ammonium bicarbonate containing 0.4 µg of MS-grade trypsin (Thermo Scientific, 90057). Trypsinization happened overnight at 37 °C with rotation, and the reactions were quenched using 1 µL of MS-grade formic acid (Fisher Scientific, A117-50). The resulting peptide-containing solution was filtered through a 0.22 µM spin filter (Corning, 8160) before mass spectrometry analysis.

General western blotting procedure

Gel electrophoresis was performed using 4–15% Bio-Rad Criterion TGX precast midi gels (5671084, 5671085), Bio-Rad Criterion Vertical midi-format electrophoresis cell (1656001), and Bio-Rad PowerPac Basic Power Supply (1645050). After electrophoresis, gels were transferred to nitrocellulose membrane using iBlot 2 gel transfer device (Thermo Scientific, IB23001) or to 0.45 µm nitrocellulose membrane (Bio-Rad, 1620115) through wet transfer. The membranes were then washed with Milli-Q water and blocked in blocking buffer (3% bovine serum albumin (BSA) in 1× 0.05% Tween 20 in tris-buffered saline (TBST) ()) for 1 h at room temperature with gentle shaking. Primary antibody was prepared in blocking buffer describe above overnight at 4 °C with gentle agitation. Membranes were washed 3× with TBST before incubating with secondary antibody solution (1:10,000) in blocking buffer for 1 h at room temperature with gentle shaking. The stained blots were again washed 3× with TBST before imaging with the Image Studio v5.2 software on LI-COR Odyssey CLx scanner in the 700 nm and 800 nm channels.

Streptavidin enrichment for TMT proteomics and mass spectrometry analysis

Procedures following ESR1-CfaN photolabeling experiment for TMT proteomics, mass spectrometry analysis, and data processing are executed as previously described[32]. Briefly, protein concentration was normalized across all experimental replicates and diluted to 1 mg/mL with binding buffer (25 mM Tris, 150 mM NaCl, 0.25% v/v NP-40, pH = 7.5). 1 mL of each sample was incubated with 125uL of prewashed Strepavidin Mag Sephrose beads (Cytiva, 28985799) for overnight at 4 °C with end-over-end rotation. The beads were then washed with 3× 500 µL of 1% SDS in DPBS, 2× 500 µL of 1 M NaCl in DPBS, 1× 500 µL of 10% EtOH in DPBS.

Following streptavidin enrichment, the beads were resuspended in 300 µL of PBS and transferred to a new 1.5 ml LoBind tube. The supernatant was removed and the beads were washed with 3× PBS (0.5 ml) and 3× ammonium bicarbonate (100 mM). The beads were resuspended in 500 µl of 3 M urea in PBS and 25 µl of 200 mM dithiothreitol in 25 mM NH_4HCO_3 was added. The beads were incubated at 55 °C for 30 min. Subsequently, 30 µl of 500 mM iodoacetamide in 25 mM NH_4HCO_3 was added and incubated for 30 min at room temperature in the dark. The supernatant was removed and the beads washed with 3× 0.5 ml of DPBS and 6× 0.5 ml of triethyl ammonium bicarbonate (TEAB, 50 mM). The beads were resuspended in 0.5 ml of TEAB (50 mM) and transferred to a new protein LoBind tube. The beads were resuspended in 40 µl of TEAB (50 mM), 1.2 µl of trypsin (1 mg/mL in 50 mM acetic acid) was added and the beads incubated overnight with end-over-end rotation at 37 °C. After 16 h, a further 0.8 µl of trypsin was added and the beads were incubated for an extra 1 h at 37 °C. Meanwhile, TMT-10-plex label reagents (0.8 mg) (Thermo) were equilibrated to room temperature and diluted with 40 µl of anhydrous acetonitrile (Optima grade; 5 min with vortexing) and centrifuged. A total of 40 µl of each TMT reagent was added to the appropriate sample. The reaction was incubated for 2 h at room temperature. The samples were quenched with 8 µl of 5% hydroxylamine and incubated for 15 min. The samples were pooled in a new Protein LoBind tube and acidified with TFA (16 µl, Optima). Mass spectra were obtained using an Orbitrap Fusion Lumos mass spectrometer at Princeton Proteomics Facility. TMT-labeled peptides were dried down in a SpeedVac, redissolved in 300 µl of 0.1% TFA in water and fractionated into eight fractions using the Pierce High pH Reversed-Phase Peptide Fractionation Kit (no. 84868). Resulting MS/MS/MS data were searched in FragPipe against the Uniprot human protein database containing common contaminants. The proteinGroups.txt file was subsequently imported into Perseus (https://maxquant.net/perseus/). The data were then filtered on the basis of the following criteria, 'only identified by site', 'reverse' and 'potential contaminant'. The resulting data were log2-transformed and median normalization was performed. FDR-corrected P values were determined by a two-sample t-test following the Benjamini–Hochberg procedure. The data were visualized by plotting as a volcano plot.

Label-free mass spectrometry analysis and data processing

Data-independent acquisition (DIA) in conjunction with label-free proteomics was conducted using a Bruker nanoElute LC connected to a TimsTOF Pro 2 mass spectrometer. ~100 ng of peptides were injected for each sample, with first loading onto a trap column (C18 Pepmap; 5 µm particle size, 5 mm length, 300 µm internal diameter), then separated by an analytical column (PepSep C18; 1.9 µm particle size, 100 mm length, 75µm internal diameter). Elution of peptides was achieved using acetonitrile/water gradient at a column temperature of 50 °C (buffer A = 0.1% formic acid in water, buffer B = 0.1% formic acid

in acetonitrile; flow rate = 0.5 µL/min, gradient starts at 2% buffer B and increase to 35% buffer B in 20 min, then increase to 95% buffer B in 0.5 min, then hold at 95% buffer B for 2.25 min). Scans were performed in positive ion mode with dia-PASEF (parallel accumulation serial fragmentation) mode over a m/z range of 100–1700 with a ramp time of 100 ms, accumulation time of 100 ms, a duty cycle of 100%, ramp rate at 9.43 Hz, and MS averaging set to 1. Absolute thresholds were set to 5000 for mobility peaks, and 10 for MS peaks. Bruker Compass HyStar v.6.2 was used for data collection.

Global proteomics as well as nuclear native IP-MS raw data were processed using DIA-NN 1.8.1. CfaC-ESR1 uMap raw data were processed using DIA-NN 2.0. The following parameters were used for all label-free proteomics data processing: trypsin/P digestion, three missed cleavages, three maximum variable modifications, N-term M excision, Oxidation (M), Acetylation (M), and C-carbamidomethylation, peptide length range of 7–30, precursor charge range 1–4, m/z range 300–1800, fragment ion range 200–1800, mass accuracy and MS accuracy set at 10, precursor false discovery rate (FDR) at 1%; the program was set to use isotopologues, match between runs (MBR), no shared spectra, and heuristic protein inference. An in silico spectral library was generated with methods previously described. The DIA-NN processed report.pg file was further analyzed using Perseus (v.2.0.7.0) with the following procedures: intensities as "main", and all other categories as "categorical"; intensities transformed by log2, each replicate annotated as conditions (DMSO, E2, Fulv), normalization achieved through median subtraction, and volcano plots generated using *t*-test for statistical significance. All volcano plots were plotted with GraphPad Prism 10. Heatmaps were generated using Morpheus (https://software.broadinstitute.org/morpheus/). Gene ontology analysis was performed using Metascape (https://metascape.org)[41].

MCF7 native nuclear co-IP

MCF7 WT cells were cultured in phenol-red free DMEM supplemented with 10% charcoal-stripped FBS, 1% L-glutamine, 1% penicillin-streptomycin and pre-treated with 10 µM of TAK-243 for 1 h prior to co-treatment with 100 nM of the corresponding drugs. Cells were harvested and washed with DPBS twice. The cells were homogenized using a Dounce homogenizer in RSB buffer (10 mM Tris, 15 mM NaCl, 1.5 mM $MgCl_2$) containing 1× protease inhibitor cocktail (Roche, 11836145001) and 100 nM of the drug. The nucleus was pelleted at 400 × *g* for 5 min and lysed using cell lysis buffer (Cell Signaling Technology, 9803S) with Benzonase nuclease (Sigma-Aldrich, E8263) and 100 nM of the drug. Protein A Magnetic Beads (Thermo Scientific, 88846) were washed with 500 µL cell lysis buffer. 400 µg of lysate was then added to the beads. They were incubated at room temperature for 20 min and pelleted on a magnetic rack. To the supernatant, Rabbit IgG Antibody (Cell Signaling Technology, 2729S) or ERα Antibody (Cell Signaling Technology, D8H8) were added following the manufacturer's instructions. The mixture was incubated overnight with rotation at 4 °C. On the second day, the beads were washed with cell lysis buffer and mixed with the immunocomplex solution. The mixture was incubated at room temperature with rotation for 20 min. The beads were pelleted on a magnetic rack and washed with cell lysis buffer mix three times. For each sample, 30 µL of 1X Laemmli (Biorad 1610747) supplemented with 10 mM DTT was added. The samples were heated at 95 °C for 10 min with shaking at 700 rpm. The supernatant was collected for proteomics SP3 cleanup.

Global proteomics

MCF7 cells were cultured in no phenol red DMEM supplemented with 10% charcoal-stripped FBS, 1% penicillin-streptomycin and 1% L-glutamine for three days before pretreated with 10 µM TAK-243 for 1 h and co-treatment of 10 µM TAK-243 and 100 nM estradiol or fulvestrant for 4 h to replicate photolabeling conditions. After harvesting, cells were washed twice with DPBS and once with RSB buffer described previously. 10 strokes were used to homogenize the cells using Dounce homogenizer in RSB buffer, and the resulting nuclear pellets were lysed using RSB buffer supplemented with 1% Triton X-100 and 50 U/mL Benzonase nuclease. The pellets were incubated on ice for 10 min before sonication at 35% intensity for 10 s. After centrifugation at 18,000 × *g* for 15 min at 4 °C, the resulting supernatant was quantified using BCA and carried through SP3 cleanup for proteomics analysis.

SP3 proteomics sample preparation

The SP3 sample preparation protocol was adapted from protocol published by Hughes et al.[58]. Briefly, the samples were treated with 15 mM iodoacetamide (IAA; Sigma-Aldrich, I6125) for 30 min at room temperature in the dark. It is then quenched with 20 mM dithiothreitol (DTT; Millipore-Sigma, 3860) for 15 min at room temperature. The prepared lysates were diluted using freshly prepared reconstitution solution (50 mM HEPES, pH 8, 1% (wt/vol) SDS, 1% (vol/vol) Triton X-100, 1% (vol/vol) NP-40, 1% (vol/vol) Tween 20, 1% (wt/vol) deoxycholate, 5 mM EDTA, 50 mM NaCl, 1% (vol/vol) glycerol, 1× Roche cOmplete protease inhibitor, and 5 mM DTT). The SP3 beads are 1:1 mixture of Sera-Mag SeedBeads (GE Healthcare, cat. no. 45152105050250 and cat. no. 65152105050250). The lysates were incubated with the SP3 beads and ethanol at 24 °C for 5 min at 1000 r.p.m to induce binding of the protein to the beads. The beads were then washed with 80% ethanol with mixing for three times. The beads were resuspended in 100 mM ammonium bicarbonate (Sigma-Aldrich, 09830) with 0.4 µg MS-grade trypsin (Thermo Fisher Scientific, 90057) per sample in Optima grade water. The mixture is sonicated in a water bath for 30 s and pipette-mixed. It is then incubated at 37 °C for 18 h in a ThermoMixer at 1000 r.p.m for 18 h for digestion. The reaction was quenched using 1 µL Optima LC–MS formic acid (Thermo Fisher Scientific, A117-50). The supernatants were passed through a 0.22-µm spin filter column (Corning, 8160) before being transferred to an LC–MS vial for proteomics analysis.

Senescence β-galactosidase staining

SASP staining was performed using Beta Galactosidase Staining Kit (Abcam, ab65351), following the manufacturer's suggestion. Briefly, the cells were fixed using fixation solution for 10 min at room temperature. The staining solution mix was made using 1% staining supplement and 5% 20 mg/mL x-gal solution in the staining solution. The cells were incubated with the staining solution mix overnight at 37 °C. The cells were imaged under a light microscope.

CUT&RUN sample preparation

MCF7 cells were treated with DMSO, 100 nM estradiol, or 100 nM Fulvestrant for 45 min. Each treatment was conducted in duplicates. H3K4Me3 and Rabbit IgG Isotype were used as the positive and negative control respectively. The samples were prepared using CUT&RUN Assay Kit (Cell Signaling Technology, 86652S) following the manufacturer's instructions. Briefly, the cells were harvested using TrypLE Express (Gibco, 12604013) and washed with 1X Wash buffer with spermidine and protease inhibitor cocktail twice. Concanavalin A Magnetic Beads were washed with Concanavalin A Bead Activation Buffer twice and resuspended in the buffer. 10 µL of activated Concanavalin A Magnetic Beads was used for each sample. The samples were mixed and incubated for 5 min at room temperature. The beads were pelleted, and its liquid removed. Then, 100 µl of Antibody Binding Buffer with spermidine, protease inhibitor cocktail and digitonin was added to each reaction. The ESR1 (Cell Signaling Technology, D8H8), H3K4Me3 (Cell Signaling Technology, 9751T), and Rabbit IgG Isotype (Cell Signaling Technology, 66362S) antibodies were added to the samples according to the manufacturer's instructions. The samples were incubated at 4 °C for 2 h. The samples were then washed with Digitonin Buffer and mixed with pAG-MNase. The mixture was incubated at 4 °C for 1 h. After incubation, the samples were washed with

Digitonin Buffer twice and pre-cooled on ice for 5 min. The pAG-MNase was activated by mixing in 3 μl cold Calcium Chloride. The digestion was conducted at 4 °C for 30 min. The reaction was stopped by adding 1× Stop Buffer (from 4× Stop Buffer, Digitonin Solution, and RNAse A). The samples were incubated at 37 °C for 10 min and centrifuged at 4 °C for 2 min at 16,000 × *g*. The supernatant was purified using spin columns (Cell Signaling Technology, 14209S) according to the manufacturer's instructions.

For the library preparation, NEBNext Ultra II DNA Library Prep with Purification Beads (New England Biolabs, E7103S) and NEBNext Multiplex Oligos for Illumina (E6440S) were used. The library was prepared using the standard steps of end-repair, adapter ligation. The adapters were diluted 10 fold to avoid excess adapter dimerization formation. The adapter ligated DNA was cleaned up without size selection and PCR enriched. The PCR product was cleaned up, and then quantified and checked using Qubit 4 Fluorometer (Thermo Fisher Scientific) and Bioanalyzer (Agilent 2100). The quality of the library was checked using the Agilent 4200 TapeStation, and preliminarily sequenced on the Illumina MiniSeq to confirm pooling uniformity. Final sequencing was performed on the Illumina NextSeq2000 using PE 161 bp reads at ~25 M reads per sample.

CUT&RUN data analysis

The data was analyzed on the local instance of Galaxy set up by the Princeton Lewis-Sigler Institute Bioinformatics Group[59]. The adapter sequences, low-quality ends (phred score <30), and reads shorter than 15 nt were trimmed using Trim Galore![60]. The trimmed sequences were aligned to human reference genome hg38 (Dec 2013) using Bowtie2[61]. The aligned sequences were filtered to remove mitochondria DNA and non-proper pairs using BamTools[62]. The duplicate reads were filtered using Picard MarkDuplicates[63]. The peaks were found using MACS2 with extension size 200 and shift size −100 and a q-value cutoff at 0.05[64]. The DNA binding motifs were discovered using MEME-ChIP and matched against known motifs using Tomtom from the MEME suite[65]. The peaks were annotated using ChIPSeeker[66]. HOMER version 5.1 was used to identify top known DNA binding motifs[67]. DiffBind version 3.12.0 was used to calculate differential DNA binding occupancy[68].

HEK293T HA-ESR1 transfection co-IP

Cells were transfected on the day after seeding. For each 15 cm plate, 15 μg HA-ESR1-pcDNA3.1(+) or pcDNA3.1(+) Expression Vector (Invitrogen, V79020) plasmid was used. The plasmids were mixed with 2.5 mL Opti-MEM (Gibco, 31985062). For each sample, 45 μL Lipofectamine 2000 (Invitrogen, 11668027) was mixed with 2.5 mL Opti-MEM. The two mixtures were incubated for 5 min and then mixed together. The Lipofectamine-DNA mixture was incubated for 20 min and added to the cell culture. On the second day, the media was changed to hormone free media. The cells were dosed on the following day with 10 μM TAK243 for 1 h before harvesting. The cell lysates were generated using cell lysis buffer (Cell Signaling Technology, 9803S) with protease inhibitor cocktail (Roche, 11836145001) in 100 nM of the drug. For each condition, 1.5 mg lysate was used. 25 μL Pierce Anti-HA Magnetic Beads (Thermo Scientific, 88836) were washed with the complete cell lysis buffer twice. The lysates were added to the beads and incubated at 4 °C overnight with rotation. After incubation, the beads were washed with the complete lysis buffer three times. The proteins were eluted from the beads with 1× Laemmli (Biorad, 1610747). The beads were heated at 95 °C for 10 min with shaking at 700–800 rpm. The supernatants were saved and 10% volume of β-mercaptoethanol were added. The samples were heated at 95 °C for 5 min with shaking at 700–800 rpm. For the input, 20 μg lysate was used for each sample, mixed with Laemmli supplemented with β-mercaptoethanol and shaked at 95 °C, 700–800 rpm for 10 min.

Fluorescence recovery after photobleaching (FRAP)

7×10^4 MCF7 cells were seeded in each well of a 24 well glass bottom plate coated with poly-L-lysine (EMD Millipore, A-005-C). On the second day, the knockdown cells were first transfected with scramble siRNA (Invitrogen, 4390843), siATRX (Dharmacon, L-006524-00-0005), or siDAXX (Dharmacon, L-004420-00-0005). For each well, 6 pmol siRNA was mixed with 50 μL Opti-MEM and 1.2 μL Lipofectamine RNAiMAX (Invitrogen, 13778150). The mixture was incubated for 5 min at room temperature before adding to the media. After 4 h, the cells were transfected with eGFP-ESR1 plasmid (Addgene, #28230) using Lipofectamine 3000 Reagent (Invitrogen, L3000015). For each well, 300 ng of plasmid was mixed with 50 μL Opti-MEM, 0.9 μL Lipo3000, and 0.6 μL p3000. The mixture was incubated at room temperature for 15 min and added to the media. On the second day, the media was changed into hormone free media. 10 μM ML792 is added for a 24-h treatment. The cells were treated with the DMSO or fulvestrant on the following day and imaged using NIS Elements AR v4.60.00 software on a Nikon A1R-Si HD confocal microscope. The cells were bleached using a 405 nm laser.

Cell viability assay

The siRNA, DMSO, Fulvestrant, or ML792 were added to the cells the day after seeding. On day 4, the media was refreshed with the same concentration of siRNA and drug. On day 8, the cell viability was done using ATPlite 1step Luminescence Assay System (Revvity Health Sciences, 6016736). The plate was warmed to room temperature and the media was changed to DPBS. 100 μL ATPLite 1step reagent was added to each well and shaked for 2 min at 700 rpm. The plate was dark adapted for 10 min and the luminescence was measured using a BioTek Gen5 v2.05 plate reader.

Senescence induction

MCF7 cells were plated into 6 well plates with DMEM with phenol red supplemented with 10% FBS and 1% penicillin-streptavidin at the following densities: 0.008×10^6 for DMSO and 1 μM E2 for 24 and 48 h, 0.2×10^6 for 1 μM Fulv for 24 and 48 h, and 0.4×10^6 for 20 μM Etoposide for 48 h. Dosing was performed 24 h after plating with fresh media, and cells were used for beta-galactosidase staining or harvested for western blot or flow cytometry 8 days after plating.

Flow cytometry

Harvested cells were washed twice with DPBS and once with freshly prepared 1× Annexin V binding buffer (10 mM HEPES, 140 mM NaCl, 2.5 mM $CaCl_2$, pH 7.4, sterile filtered). Cells were stained with 5 μL Annexin V-Alexa Fluor 647 (Invitrogen, A23204) for 15 min at room temperature protected from light. The stained cells were washed again with 1× Annexin V binding buffer before fixed and permeabilized using eBioScience Foxp3/Transcription Factor Staining Buffer Kit (Invitrogen, 00-5523-00) per manufacturer's directions. Briefly, a 1:3 Fix/Perm concentrate: Fix/Perm Diluent was used to fix and permeabilize the cells at 4 °C for 30 min in dark. 2× volume of 1× Perm buffer (made from 10× Perm buffer from the kit) was directed added to the cell mixture, with the resulting mixture being centrifuged to discard the supernatant. The pellets were stained with 5 μL Ki67-PE (BD Pharmingen, 556027) and 10 μg/mL DAPI in 1× Perm buffer for 1 h at room temperature protected from light. The stained cells were washed twice with 1× Perm buffer and resuspended in 2% FBS in DPBS before flow cytometric analysis using the FACSymphony A3 instrument (BD Biosciences) at Princeton University Flow Cytometry Resource Facility. The Annexin V-Alexa647, Ki67-PE, and DAPI were excited with 637, 561, and 355 nm lasers, respectively, and emitted fluorescence was collected via 670/30, 586/15, and 450/50 bandpass filters, respectively.

Confocal and stimulated emission depletion (STED) microscopy

MCF7 or T47D cells were plated into glass bottom 24 well plates (Ibidi, 82427) precoated with poly-L-lysine (bio-techne, 3438-100-01). For the truncation STED microscopy, U2OS cells were transfected with the corresponding plasmid using Lipofectamine (Invitrogen, 11668019). The cells were treated with 10 μM TAK243 for 1 h followed by 4 h treatment of 100 nM fulvestrant. After treatment with the corresponding drugs, cells were fixed using 4% paraformaldehyde in DPBS for 15 min at room temperature and washed twice with DPBS. Subsequently, cells were permeabilized with 0.1% Triton X-100 in DPBS for 15 min at room temperature, washed twice with DPBS, and blocked with 3% bovine serum albumin (BSA) in DPBS for 1 h at room temperature. Samples after blocking were treated with the corresponding primary antibodies at concentrations noted by vendor overnight at 4 °C in 3% BSA in DPBS, and stained with secondary antibodies necessary for confocal or STED microscopy after washing with 0.2% Tween 20 in DPBS (PBST) three times. The final stained samples were washed again using PBST, and preserved in DPBS during imaging at Princeton University Core Confocal Imaging Facility. Confocal images were acquired using Nikon A1R-Si HD microscope with digital micromirror device, and STED images were acquired using Nikon A1R-STED confocal microscope with stimulation emission depletion detector.

Fractionation analysis

MCF7 cells were cultured as described and harvested using TrypLE Express. Cells were washed twice using DPBS, and fractionation was performed using Thermo Scientific Subcellular Protein Fractionation Kit for Cultured Cells (Thermo, 78840) with manufacturer's protocols. Cytosolic fraction, soluble nuclear fraction, and chromatin (insoluble) fraction were isolated using the kit, and the cytosolic and soluble nuclear fractions were further cleared with centrifugation at 16,000 × *g* for 5 min at 4 °C. The resulting lysates were subjected to western blotting analysis.

Statistics and reproducibility

Statistical tests are used as indicated in this study. Experiments are performed in biological triplicates unless otherwise stated.

Reporting summary

Further information on research design is available in the Nature Portfolio Reporting Summary linked to this article.

Data availability

The data supporting the findings of this study are available within the paper and its Supporting Information. Source data are provided with this paper. The CUT&RUN data generated in this study have been deposited in the NCBI GEO database under accession number GSE331140. The proteomics data generated in this study have been deposited in the MassIVE database under accession number MSV000101862 [https://massive.ucsd.edu/ProteoSAFe/dataset.jsp?task=a0a19ff7c8464daa9de101bf2066e1d7]. Analyzed sequencing and proteomics data are also included in the supplementary data. Source data are provided with this paper.

References

1. Cook, D. et al. Lessons learned from the fate of AstraZeneca's drug pipeline: a five-dimensional framework. *Nat. Rev. Drug Discov.* **13**, 419–431 (2014).
2. Mechanism matters. *Nat. Med.* **16**, 347–347 (2010).
3. Yamaguchi, S., Kaneko, M. & Narukawa, M. Approval success rates of drug candidates based on target, action, modality, application, and their combinations. *Clin. Transl. Sci.* **14**, 1113–1122 (2021).
4. Kiriiri, G. K., Njogu, P. M. & Mwangi, A. N. Exploring different approaches to improve the success of drug discovery and development projects: a review. *Future J. Pharm. Sci.* **6**, 27 (2020).
5. Miner, J. & Hoffhines, A. The discovery of aspirin's antithrombotic effects. *Tex. Heart Inst. J.* **34**, 179–186 (2007).
6. Rehman, W., Arfons, L. M. & Lazarus, H. M. The rise, fall and subsequent triumph of thalidomide: lessons learned in drug development. *Ther. Adv. Hematol.* **2**, 291–308 (2011).
7. Mateo, J., Ong, M., Yap, T. A. & de Bono, J. S. Opportunities and pitfalls of targeted therapeutic combinations in solid tumors. *Am. Soc. Clin. Oncol. Educ. Book* 670–674 (2012).
8. Patel, H. K. & Bihani, T. Selective estrogen receptor modulators (SERMs) and selective estrogen receptor degraders (SERDs) in cancer treatment. *Pharmacol. Therapeutics* **186**, 1–24 (2018).
9. Bross, P. F., Cohen, M. H., Williams, G. A. & Pazdur, R. FDA drug approval summaries: fulvestrant. *Oncologist* **7**, 477–480 (2002).
10. Neupane, N. et al. Oral SERD, a novel endocrine therapy for estrogen receptor-positive breast cancer. *Cancers* **16**, 619 (2024).
11. Bardia, A. et al. The oral selective estrogen receptor degrader GDC-0810 (ARN-810) in postmenopausal women with hormone receptor-positive HER2-negative (HR+/HER2–) advanced/metastatic breast cancer. *Breast Cancer Res Treat.* **197**, 319–331 (2023).
12. US National Library of Medicine. ClinicalTrials.gov. A Study of GDC-0810 Versus Fulvestrant in Postmenopausal Women With Advanced or Metastatic Breast Cancer Resistant to Aromatase Inhibitor (AI) Therapy (HydranGea). https://clinicaltrials.gov/study/NCT02569801 (accessed 30 June 2026) (2021).
13. Chandarlapaty, S. et al. An open-label phase I study of GDC-0927 in postmenopausal women with locally advanced or metastatic estrogen receptor–positive breast cancer. *Clin. Cancer Res.* **29**, 2781–2790 (2023).
14. Tolaney, S. M. et al. AMEERA-3: randomized phase II study of amcenestrant (oral selective estrogen receptor degrader) versus standard endocrine monotherapy in estrogen receptor–positive, human epidermal growth factor receptor 2–negative advanced breast cancer. *JCO* **41**, 4014–4024 (2023).
15. Robertson, J. F. R. et al. A randomized, open-label, presurgical, window-of-opportunity study comparing the pharmacodynamic effects of the novel oral SERD AZD9496 with fulvestrant in patients with newly diagnosed ER+ HER2– primary breast cancer. *Clin. Cancer Res.* **26**, 4242–4249 (2020).
16. Guan, J. et al. Therapeutic ligands antagonize estrogen receptor function by impairing its mobility. *Cell* **178**, 949–963.e18 (2019).
17. Charn, T. H. et al. Genome-wide dynamics of chromatin binding of estrogen receptors α and β: mutual restriction and competitive site selection. *Mol. Endocrinol.* **24**, 47–59 (2010).
18. Candelaria, N. R., Liu, K. & Lin, C.-Y. Estrogen receptor alpha: molecular mechanisms and emerging insights. *J. Cell. Biochem.* **114**, 2203–2208 (2013).
19. Cheng, A. S. L. et al. Combinatorial analysis of transcription factor partners reveals recruitment of c-MYC to estrogen receptor-α responsive promoters. *Mol. Cell* **21**, 393–404 (2006).
20. Jeong, K. W., Lee, Y.-H. & Stallcup, M. R. Recruitment of the SWI/SNF chromatin remodeling complex to steroid hormone-regulated promoters by nuclear receptor coactivator flightless-I. *J. Biol. Chem.* **284**, 29298–29309 (2009).
21. Hanstein, B. et al. p300 is a component of an estrogen receptor coactivator complex. *Proc. Natl. Acad. Sci. USA* **93**, 11540–11545 (1996).
22. Toyama, T. & Iwase, H. p33ING1b and estrogen receptor (ER) alpha. *Breast Cancer* **11**, 33–37 (2004).
23. Nishide, G. et al. Zooming into gene activation: estrogen receptor α dimerization and DNA binding visualized by high-speed atomic force microscopy. *ACS Nano* **19**, 15395–15410 (2025).
24. Paakinaho, V. et al. Single-molecule analysis of steroid receptor and cofactor action in living cells. *Nat. Commun.* **8**, 15896 (2017).

25. Sharp, Z. D. et al. Estrogen-receptor-α exchange and chromatin dynamics are ligand- and domain-dependent. *J. Cell Sci.* **119**, 4101–4116 (2006).
26. Klinge, C. M., Jernigan, S. C., Mattingly, K. A., Risinger, K. E. & Zhang, J. Estrogen response element-dependent regulation of transcriptional activation of estrogen receptors α and β by coactivators and corepressors. *J. Mol. Endocrinol.* **33**, 387–410 (2004).
27. Traboulsi, T., El Ezzy, M., Dumeaux, V., Audemard, E. & Mader, S. Role of SUMOylation in differential ERα transcriptional repression by tamoxifen and fulvestrant in breast cancer cells. *Oncogene* **38**, 1019–1037 (2019).
28. Agbo, L., Blanchet, S. A., Kougnassoukou Tchara, P.-E., Fradet-Turcotte, A. & Lambert, J.-P. Comprehensive interactome mapping of nuclear receptors using proximity biotinylation. In *Proteomics in Systems Biology: Methods and Protocols* (ed. Geddes-McAlister, J.) 223–240 (Springer US, 2022).
29. Rega, C. et al. Exploring the spatial landscape of the Estrogen Receptor proximal proteome with antibody-based proximity labeling. *Mol. Cell. Proteom.* **23**, 100702 (2024).
30. Geri, J. B. et al. Microenvironment mapping via Dexter energy transfer on immune cells. *Science* **367**, 1091–1097 (2020).
31. Trowbridge, A. D. et al. Small molecule photocatalysis enables drug target identification via energy transfer. *Proc. Natl. Acad. Sci. USA* **119**, e2208077119 (2022).
32. Seath, C. P. et al. Tracking chromatin state changes using nanoscale photo-proximity labelling. *Nature* **616**, 574–580 (2023).
33. Oakley, J. V. et al. Radius measurement via super-resolution microscopy enables the development of a variable radii proximity labeling platform. *Proc. Natl. Acad. Sci. USA* **119**, e2203027119 (2022).
34. DepMap: The Cancer Dependency Map Project at Broad Institute. https://depmap.org/portal/ (2026).
35. Arafeh, R., Shibue, T., Dempster, J. M., Hahn, W. C. & Vazquez, F. The present and future of the Cancer Dependency Map. *Nat. Rev. Cancer* **25**, 59–73 (2025).
36. Fu, A. et al. Nuclear p62 condensates stabilize the promyelocytic leukemia nuclear bodies by sequestering their ubiquitin ligase RNF4. *Proc. Natl. Acad. Sci. USA* **121**, e2414377121 (2024).
37. Pankiv, S. et al. Nucleocytoplasmic shuttling of p62/SQSTM1 and its role in recruitment of nuclear polyubiquitinated proteins to promyelocytic leukemia bodies. *J. Biol. Chem.* **285**, 5941–5953 (2010).
38. Corpet, A. et al. PML nuclear bodies and chromatin dynamics: catch me if you can!. *Nucleic Acids Res.* **48**, 11890–11912 (2020).
39. Hofmann, T. G. & Will, H. Body language: the function of PML nuclear bodies in apoptosis regulation. *Cell Death Differ.* **10**, 1290–1299 (2003).
40. Lallemand-Breitenbach, V. & de Thé, H. PML nuclear bodies. *Cold Spring Harb. Perspect. Biol.* **2**, a000661 (2010).
41. Zhou, Y. et al. Metascape provides a biologist-oriented resource for the analysis of systems-level datasets. *Nat. Commun.* **10**, 1523 (2019).
42. Vernier, M. et al. Regulation of E2Fs and senescence by PML nuclear bodies. *Genes Dev.* **25**, 41–50 (2011).
43. Topacio, B. R. et al. Cyclin D-Cdk4,6 drives cell-cycle progression via the retinoblastoma protein's C-terminal helix. *Mol. Cell* **74**, 758–770.e4 (2019).
44. Hilmi, K. et al. Role of SUMOylation in full antiestrogenicity. *Mol. Cell Biol.* **32**, 3823–3837 (2012).
45. Horwitz, K. B., Mockus, M. B. & Lessey, B. A. Variant T47D human breast cancer cells with high progesterone-receptor levels despite estrogen and antiestrogen resistance. *Cell* **28**, 633–642 (1982).
46. El-Masry, O. S., Brown, B. L. & Dobson, P. R. M. AMPK activation of apoptotic markers in human breast cancer cell lines with different p53 backgrounds: MCF-7, MDA-MB-231 and T47D Cells. *Asian Pac. J. Cancer Prev.* **20**, 3763–3770 (2019).
47. Kumar, R. et al. The dynamic structure of the estrogen receptor. *J. Amino Acids* **2011**, 812540 (2011).
48. Skene, P. J., Henikoff, J. G. & Henikoff, S. Targeted in situ genome-wide profiling with high efficiency for low cell numbers. *Nat. Protoc.* **13**, 1006–1019 (2018).
49. Bjornstrom, L., Kilic, E., Norman, M., Parker, M. G. & Sjoberg, M. Cross-talk between Stat5b and estrogen receptor-alpha and -beta in mammary epithelial cells. *J. Mol. Endocrinol.* **27**, 93–106 (2001).
50. Siersbæk, R. et al. IL6/STAT3 signaling hijacks ER enhancers to drive breast cancer metastasis. *Cancer Cell* **38**, 412–423.e9 (2020).
51. Fracassi, C., Simoni, M., Uggè, M., Morelli, M. J. & Bernardi, R. PML is a constitutive component of chromatin domains enriched in repetitive elements and duplicated gene clusters in cancer cells. *Heliyon* **10**, e36499 (2024).
52. Stergachis, A. B. et al. Exonic transcription factor binding directs codon choice and impacts protein evolution. *Science* **342**, 1367–1372 (2013).
53. Fiszbein, A., Krick, K. S., Begg, B. E. & Burge, C. B. Exon-mediated activation of transcription starts. *Cell* **179**, 1551–1565.e17 (2019).
54. Wang, L. & Han, T. Pharmacologic induction of ERα SUMOylation disrupts its chromatin binding. *ACS Chem. Biol.* **19**, 2383–2392 (2024).
55. Tsai, J. M. et al. UBR5 forms ligand-dependent complexes on chromatin to regulate nuclear hormone receptor stability. *Mol. Cell* **83**, 2753–2767.e10 (2023).
56. Kalinsky, K. et al. Abemaciclib plus fulvestrant in advanced breast cancer after progression on CDK4/6 inhibition: results from the phase III postMONARCH trial. *JCO* **43**, 1101–1112 (2025).
57. Burton, A. J. et al. In situ chromatin interactomics using a chemical bait and trap approach. *Nat. Chem.* **12**, 520–527 (2020).
58. Hughes, C. S. et al. Single-pot, solid-phase-enhanced sample preparation for proteomics experiments. *Nat. Protoc.* **14**, 68–85 (2019).
59. The Galaxy Community. The Galaxy platform for accessible, reproducible, and collaborative data analyses: 2024 update. *Nucleic Acids Res.* **52**, W83–W94 (2024).
60. Krueger, F. Trim Galore. Github https://github.com/felixkrueger/trimgalore (2026).
61. Langmead, B. & Salzberg, S. L. Fast gapped-read alignment with Bowtie 2. *Nat. Methods* **9**, 357–359 (2012).
62. Barnett, D. W., Garrison, E. K., Quinlan, A. R., Strömberg, M. P. & Marth, G. T. BamTools: a C++ API and toolkit for analyzing and managing BAM files. *Bioinformatics* **27**, 1691–1692 (2011).
63. Broad Institute. Picard Tools https://broadinstitute.github.io/picard/ (2026).
64. Gaspar, J. M. Improved peak-calling with MACS2. *Prepr. BioRxiv* https://doi.org/10.1101/496521 (2018).
65. Bailey, T. L., Johnson, J., Grant, C. E. & Noble, W. S. The MEME Suite. *Nucleic Acids Res.* **43**, W39–W49 (2015).
66. Yu, G., Wang, L.-G. & He, Q.-Y. ChIPseeker: an R/Bioconductor package for ChIP peak annotation, comparison and visualization. *Bioinformatics* **31**, 2382–2383 (2015).
67. Homer Software and Data Download. http://homer.ucsd.edu/homer/ (2026).
68. Stark, R. & Brown, G. D. DiffBind: Differential binding analysis of ChIP-Seq peak data. *Bioconductor* https://bioconductor.org/packages/release/bioc/html/DiffBind.html (2012).

Acknowledgements

The authors thank Xuanjia Ye and Nir Hananya from the Muir Group at Princeton University Department of Chemistry for the help in the synthesis of Ir-Cfa^{N} and providing purified Cfa^{N}-KSK-SUMO. The authors thank Gary Laevsky and Sha Wang for microscopy support at the Confocal Imaging Facility, a Nikon Center of Excellence, in the Department of Molecular Biology at Princeton University. The authors also thank Ingrid Wertz, formerly of Bristol Myers Squibb, for her valuable

guidance. Generalized schemes were created with Biorender. Protein illustrations were created with ChimeraX. We thank Phylo for providing Biomni Labs Pro access through the Phylo Academic Lab Program.

Author contributions

C.L., Z.D., C.P.S., J.W.T., and D.W.C.M. conceived this work. C.L. designed and performed all proximity labeling, global proteomics, flow cytometry, and fractionation experiments. Z.D. designed and performed all co-IP, and cell viability experiments as well as CUT&RUN data analysis. C.L. and Z.D. together designed and performed nuclear IP-MS, FRAP, STED microscopy, CUT&RUN, senescence beta-galactosidase assay, and phosphor-Rb measurements. K.D. generated stable cell lines. R.O.G. performed Illumina Sequencing. C.L., Z.D., R.O.G., K.D., C.P.S., Y.A., J.L.S., A.M.K., J.W.T., and D.W.C.M. analyzed results and contributed to experimental design. C.L., Z.D., C.P.S., J.W.T., and D.W.C.M. wrote and revised this manuscript.

Funding

The authors are grateful for financial support provided by the Princeton Catalysis Initiative, and Bristol Myers Squibb. Flow cytometry support was provided by Christina DeCoste and Jailene Garcia from Princeton Flow Cytometry Core Facility with financial support from National Institute of Health (1S10OD028592-01A1) for the FACSymphony A3 flow cytometer.

Competing interests

D.W.C.M. declares an ownership interest in the company Dexterity Pharma LLC, which has commercialized materials used in this work. R.O.G., K.D., Y.A., J.L.S., A.M.K., and J.W.T. are employees and shareholders of Bristol Myers Squibb. The other authors declare no competing interests.

Additional information

Supplementary information The online version contains supplementary material available at https://doi.org/10.1038/s41467-026-77034-w.

Correspondence and requests for materials should be addressed to Joel W Thompson or David W. C. MacMillan.

Peer review information *Nature Communications* thanks Xiulei Mo, Eneda Toska, and the other, anonymous, reviewer(s) for their contribution to the peer review of this work. A peer review file is available.